Probing the Formation of Galaxies using Lyman-Alpha Emission and Absorption

Sandy Gonçalves Morais
Mestrado em Astronomia
Departamento de Física e Astronomia
2015

Orientador
Andrew James Humphrey,
Investigador, Centro de Astrofísica da Universidade do Porto

Coorientador
Patricio Lagos,
Investigador, Centro de Astrofísica da Universidade do Porto

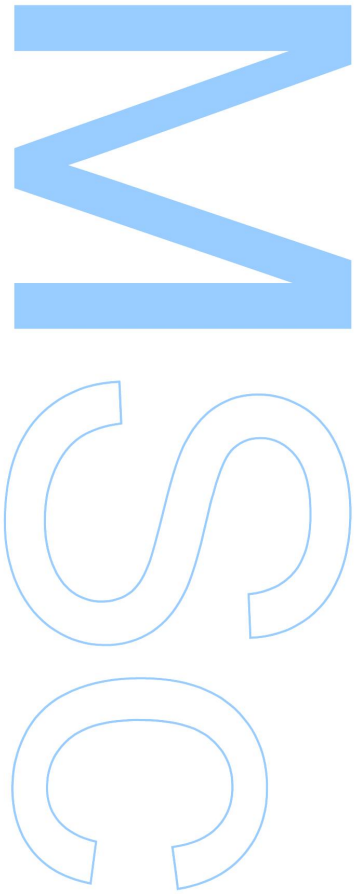

U.PORTO

FACULDADE DE CIÊNCIAS
UNIVERSIDADE DO PORTO

Todas as correções determinadas pelo júri, e só essas, foram efetuadas.

O Presidente do Júri,

Porto, _____/_____/_____

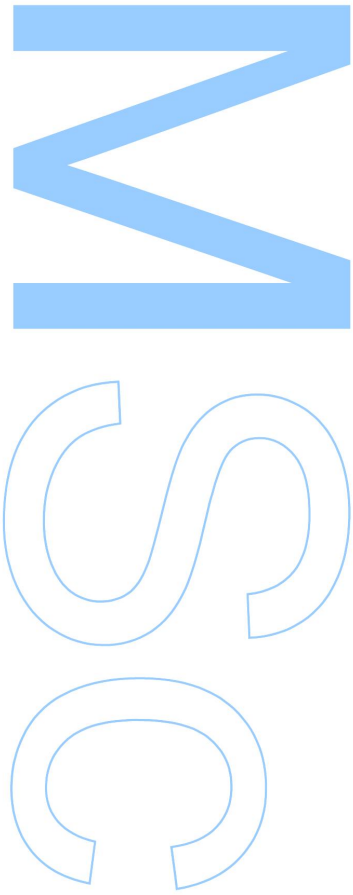

Acknowledgements

I would like to thank my supervisor Andrew Humphrey and my co-supervisor Patrício Lagos for the support they gave me to finish this thesis. Without their help it would not be possible to deliver this work. In particular, I would like to thank Andrew for all his help, patience and guidance in all the time of research and writing of this thesis.

I would also like to thank Andrew Humphrey, Montse Villar-Martín, Joël Vernet, Bob Fosbury, Andrea Cimatti, Sperello di Serego Alighieri, Marshall Cohen and Robert Goodrich for kindly making the Keck II spectroscopic data available for this project.

Thanks to all my friends for all their help and encouragement during this work. A very special thanks to my boyfriend for always cheering me up and for always believing in me.

Finally, I would like to thank my family: my parents, my godmother and especially my grandparents for supporting me throughout my entire life.

Abstract

The study of high redshift objects is important to analyze the physical conditions of the early universe and to study how galaxies form and evolve. High redshift radio galaxies and, in particular, the giant Lyα halos often found associated with them are useful to study the physical conditions and properties of the gas of what are believed to be massive galaxies in the process of formation.

There have been many previous studies of the Lyα halos of high redshift radio galaxies using the long slit technique, almost always with the slit aligned with the major axis of the radio and UV/optical emission, providing only a limited view of Lyα halos. Here, we present new spectroscopic observations of TXS 0211-122 and TXS 0828+193, taken with the long slit placed perpendicularly to the radio axis. These two radio galaxies are known to be associated with giant Lyα halos. This allows the characterization of the morphological, kinematic, and ionization properties of the gas in regions that are outside of the ionizing beams of the AGN and which are not spatially coincident with the powerful radio jets. With access to pre-existing Keck II observations taken with the long slit positioned along the radio axis we are able to make comparisons between the properties of the gas in different regions of the galaxies.

The observations of TXS 0211-122 show emission from Lyα, NV, CIV, HeII and CIII] in the direction perpendicular to the radio axis. The observations in both position angles suggest high levels of chemical enrichment of the gas. They also show that Lyα emission is being strongly absorbed and that its spatial and velocity profiles are affected by HI absorption and scattering.
In the observations with the perpendicular slit, a continuum source is detected in the northern region of the centre of the radio galaxy, close to the edge of the Lyα nebula. We suggest that this source is part of an arc-like feature surrounding the Lyα halo.
Evidence for outflowing gas is also found in TXS 0211-122. The outflow seems to be re-

stricted to the radio axis and may be due to jet-gas interactions. In the direction perpendicular to the radio axis the kinematics of HeII suggest the presence of quiescent gas.

In TXS 0828+193 a large Lyα halo is detected in the direction perpendicular to the radio axis. In this position angle, emission from NV, CIV, HeII and CIII] is also detected.
The presence of strong HeII emission and the disturbed kinematics found in Lyα, HeII and CIV in the perpendicular slit, a region that is probably not photoionized by the AGN, suggests that the gas is being ionized by shocks.
Evidence for outflowing gas, with an approximately spherical distribution is found. We suggest that we are seeing a spherical shell or bubble of expanding gas.

galaxy: formation - high redshift radio galaxies - Lyα halos - outflows

Resumo

O estudo de objetos a elevado redshift é importante para analisar as condições físicas do universo primordial e para o estudo da formação e evolução das galáxias. Rádio galáxias a elevado redshift e, em particular, os halos gigantes de Lyα que muitas vezes são encontrados associados a elas, são úteis para o estudo das condições físicas e propriedades do gás do que se pensa ser galáxias massivas em processo de formação.

Foram feitos muito estudos anteriormente acerca dos halos de Lyα associados a rádio galáxias a elevado redshift usando a técnica de fenda longa, quase sempre com a fenda alinhada com os eixos da emissão rádio e visível/UV, fornecendo uma visão limitada dos halos de Lyα. Nesta tese, apresentamos novas observações espectroscópicas de TXS 0211-122 and TXS 0828+193, feitas com a fenda longa alinhada perpendicularmente ao eixo da emissão rádio. Sabe-se que estas duas rádio galáxias estão associadas com halos gigantes de Lyα. Isto permite a caracterização das propriedades morfológicas, cinemáticas e de ionização do gás que se encontra em regiões que ficam fora dos feixes de ionização do AGN e que não coincidem espacialmente com os poderosos jatos emissores de rádio. Com acesso a observações pré-existentes, feitas com a fenda longa alinhada com os eixos de emissão rádio usando o Keck II, podemos fazer comparações entre as propriedades do gás em diferentes regiões das galáxias.

As observações de TXS 0211-122 mostram emissão de Lyα, NV, CIV, HeII e CIII] na direção perpendicular ao eixo de emissão rádio. As observações em ambos os ângulos sugerem que o gás foi enriquecido quimicamente. Também mostram que a emissão Lyα está a ser fortemente absorvida e que os perfis espacial e de velocidade da risca são afetados por absorção e dispersão devido à presença de HI.
Nas observações com a fenda na direção perpendicular, uma fonte de emissão contínua é detetada na região a norte do centro da rádio galáxia, perto do limite da nebulosa de Lyα. Sugerimos que esta fonte de emissão é parte de uma estrutura em forma de arco que

rodeia o halo de Lyα.
Também se encontram provas de que existe gás em "outflow" em TXS 0211-122. O "outflow" parece estar restrito ao eixo de emissão rádio e pode ser devido a interações entre os jatos e o gás. Na direção perpendicular ao eixo de emissão rádio a cinemática de HeII sugere a presença de gás quiescente.

Em TXS 0828+193 deteta-se um extenso halo de emissão Lyα na direção perpendicular aos eixos de emissão rádio. Neste ângulo também se deteta emissão de NV, CIV, HeII e CIII].
A presença de forte emissão de HeII e a cinemática perturbada encontrada em Lyα, HeII e CIV na posição perpendicular, uma região que provavelmente não é ionizada pelo AGN, sugere que o gás está a ser ionizado por choques.
Foram encontradas provas de que existe gás em "outflow", com uma distribuição aproximadamente esférica. Sugerimos que estamos a ver uma concha esférica ou uma bolha de gás em expansão.

galáxias: formação - rádio galáxias a elevado redshift - halos de Lyα - outflows

Contents

List of Figures

List of Tables

Chapter 1

Introduction

The study of the structure and composition of active nuclei and their hosts at high redshift is essential to understand galaxy formation and evolution.

According to the standard Λ Cold Dark Matter model it is believed that massive galaxies grow in a hierarchical manner, through the merging of smaller stellar and dark matter objects (Kauffmann and Charlot, 1998). It has been suggested that their central massive back holes grow in a similar fashion (Kauffmann and Haehnelt, 2000). Supermassive black holes (SMBHs) are found in practically all massive galaxies (e.g. Magorrian et al., 1998; Cattaneo et al., 2009), and it is believed that the evolution of galaxies and the growth of black holes is correlated. Kormendy and Richstone (1995); Magorrian et al. (1998) found that the masses of SMBHs are proportional to the masses and luminosities of their host galaxies, and Ferrarese and Merritt (2000); Gebhardt et al. (2000) found a correlation between the masses of SMBHs and the velocity dispersions of the bulges of the host galaxies.

It has been proposed that feedback from SMBHs is an essential process in the formation and evolution of galaxies. This process is assumed to regulate black hole growth and to influence the evolution of the host galaxy by supressing the cooling flows and preventing further star formation (e.g. Silk and Rees, 1998; Springel et al., 2005; Bower et al., 2006; Hopkins et al., 2006; Cano-Díaz et al., 2012). It is thought that massive galaxies experienced an early epoch of vigorous star formation terminated by a phase of active galactic nuclei (AGN) feedback (e.g. Silk and Rees, 1998; Springel et al., 2005; Bower et al., 2006; Hopkins et al., 2006). Such a phase would terminate star formation by heating and expelling significant fractions of cold gas within the host galaxy.

Massive galaxies appear to have completed most of their growth at high redshift ($z > 2$, e.g. Miley et al., 2009), therefore understanding massive galaxy evolution requires observations of active galaxies at high redshift.

1.1 HIGH REDSHIFT RADIO GALAXIES

The standard model for powerful double radio sources was first developed by Scheuer (1974) and Blandford and Rees (1974). An illustration can be seen Figure 1.1.

An AGN is located at the centre. The AGN is probably powered by the accretion of matter onto a spinning SMBH. Close to the black hole, the magnetic field becomes so strong that it forms relativistic radio-emitting plasma jets that are emitted along the spin axis of the accretion disk. The radio emission is nonthermal, produced by high energy particles moving through magnetic fields, producing synchrotron emission. The jets propagate toward the lobes which have spatial extents ranging from $\sim$ 1 kpc up to a few Mpc (Saripalli et al., 2005). The jets are usually asymmetric (which may be due to an asymmetric distribution of the gas surrounding the source, e.g. Saikia et al., 1995), often only one is observed, and in sources with two jets one is usually brighter than the other (Sparke and Gallagher, 2007). The hotspots are regions of shocked gas due to the interaction between the jets and the intergalactic medium. The shocked material flows back towards the galaxy and forms a cocoon. The expansion of the cocoon drives a bow shock outward.

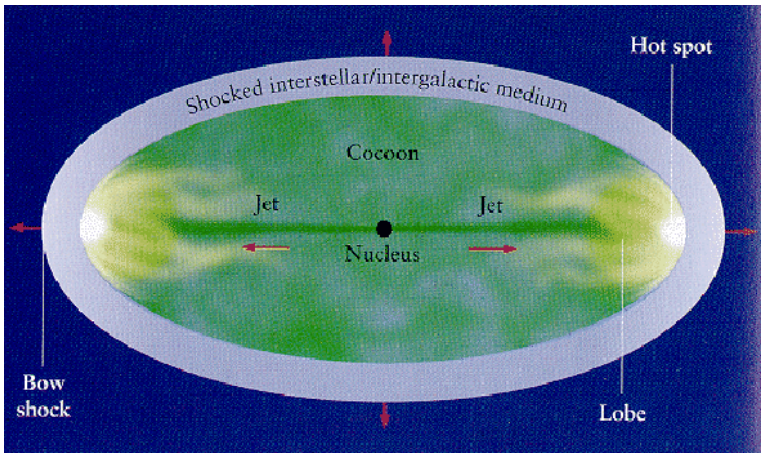

Figure 1.1: Representation of the global characteristics of powerful double lobed radio sources. Diagram taken from Begelman and Rees (1996).

High redshift radio galaxies ($z > 2$, hereinafter HzRGs) are useful for understanding the evolution of massive galaxies. There are several reasons for this: HzRGs are amongst

the largest, most massive and most luminous objects in the Universe (e.g. De Breuck et al., 2002; Willott et al., 2003; Rocca-Volmerange et al., 2004); near-IR and HST imaging of radio galaxies between redshifts 2 and 3 reveal clumpy morphologies, as expected if galaxies are forming through mergers and in agreement with hierarchical models of galaxy evolution (e.g. Dubinski, 1998; Springel et al., 2005); they are often found in dense cluster-type regions (e.g. McCarthy, 1993; van Ojik et al., 1996, 1997; Athreya et al., 1998; Pentericci et al., 2000; Venemans et al., 2004); they are believed to be the progenitors of massive elliptical and cD galaxies (Pentericci et al., 1999).

An interesting discovery was made in 1987. McCarthy et al. (1987); Chambers et al. (1987) found that the optical/IR continuum of 3C and 4C radio galaxies ($z \gtrsim 0.6$) were roughly aligned with the radio structures. This phenomenon is known as the alignment effect and it is common at $z \gtrsim 2$. Several models have been proposed to explain this effect (e.g. McCarthy, 1993). One of them is that the emission is dominated by light from young stars that formed due to the collapse of dense gas clouds shocked by the passage of the jet (Chambers et al., 1987; McCarthy et al., 1987; Bicknell et al., 2000). Another interpretation is that the emission could be scattered or reprocessed radiation from the AGN (Tadhunter et al., 1992).

Many powerful HzRGs are embedded in large (sometimes up to $\sim$ 200 kpc) luminous Lyα nebulae (van Ojik et al., 1997; Villar-Martín et al., 2003; Reuland et al., 2003) which have clumpy, irregular morphologies (e.g. Reuland et al., 2003), and are often aligned with the radio source axis (McCarthy et al., 1987, 1995). The origin of the nebulae is still unknown. They could represent the material from which the galaxies are forming (Reuland et al., 2003), or they could represent gas expelled from the galaxy (Röttgering and Pentericci, 1999). Various mechanisms have been proposed for exciting the emission line nebulae, including photoionization from AGNs (e.g. Fosbury et al., 1982), photoionization from stars, photoionization by X-rays emitted by shocked warm gas, collisional excitation from shocks (e.g. Bicknell et al., 2000) and scattering of Lyα photons by HI (Humphrey et al., 2013).

Two distinct kinematic regions are seen in the ionized gas halos (e.g. van Ojik et al., 1996; Röttgering and Pentericci, 1999). Nuclear turbulent gas regions, where there is evidence for outflows, and outer regions where the dominant systematic motions may be inwards. The inner regions show signs of perturbation by the jets, disturbed kinematics and have velocities dispersions higher than 1000 km s^{-1} (e.g. Tadhunter, 1991; McCarthy, 1993; van Ojik et al., 1997; Villar-Martín et al., 1999b; Inskip et al., 2002). These regions also show evidence for starburst superwinds (Zirm et al., 2005). Both the winds and the jets may exert sufficient pressure on the heated gas to drive it outwards. Usually, the outer regions of

the halos display velocity variations of a few hundred km s^{-1} and they could be the result of outflows (Nesvadba et al., 2006; Humphrey et al., 2006), rotation (van Ojik et al., 1996; Villar-Martín et al., 2006) or infall (Humphrey et al., 2007b). The jet-induced outflows could be the responsible mechanism for regulating galaxy growth and polluting the intergalactic medium with metals (e.g. Nesvadba et al., 2006).

1.2 LYMAN ALPHA

Hydrogen is the most abundant element in the Universe and it is a unique tracer of galaxy formation and evolution. The strongest UV-optical line of hydrogen is Lyα. It results from a transition between the first excited state (2 ^{2}P) and the ground state (1 ^{2}S), and has a wavelength of 1215.67Å that can be observed from the ground at z$\geq$2 due to being redshifted into the optical.

Lyα is usually the brightest emission line emitted by the Lyα halos, and thus to understand the properties of the nebulae we need to first understand the formation of the line.
Lyα is a resonance line hence its visibility is influenced by dust, neutral gas kinematics and geometry (e.g. Kunth et al., 1994; Shapley et al., 2003; Duval et al., 2014). In a medium where neutral hydrogen is present Lyα photons may be absorbed and re-emitted several times before they can escape. The long scattering path length makes Lyα photons extremely vulnerable to dust attenuation (e.g. Neufeld, 1990; Charlot and Fall, 1991; Hartmann et al., 1988). Moreover, Lyα photons may emerge far from the regions where they were produced.

1.3 THIS THESIS

The origin, gas distribution, chemical composition and the source of ionization of the gas in the extended Lyα halos are still unknown. Lyα halos may provide important information about the early stages of the formation of massive elliptical galaxies therefore the study of their properties is essential to determine how hosts of powerful radio galaxies form and evolve.

Numerous spectroscopic studies of HzRGs have been performed using the long-slit technique. In most cases the slit was aligned with the radio structures (e.g. Legrand et al., 1997;

Vernet et al., 2001; Villar-Martín et al., 2003). This is the region where the impact of jet-gas interactions and the ionizing radiation of the AGN are likely to be strongest. Spectroscopic observations in other directions would be helpful to study the properties of the regions far from the radio jets, outside the ionizing beams of the AGN.

TXS 0211-122 and TXS 0828+193 are the two radio galaxies studied in this thesis. They are known to be associated with very extended Lyα halos (Vernet et al., 2001; Villar-Martín et al., 2002, 2003). For each one we have long-slit spectra observations taken with the slit placed perpendicularly to the radio source axis. This allows the characterization of the properties of the gas in regions that are outside of the ionizing beams of the AGN, and far from the radio axis. This information will be important to understand the origin of the nebulae and their possible link with the formation of the galaxies.
With access to Keck II observations taken with the slit positioned *along* the radio axis (Vernet et al., 2001; Villar-Martín et al., 2002, 2003) comparisons between the properties of the different regions of the galaxy can be made.

This thesis is organized as follows: in Chapter 2 a description of the observations and the data reduction is presented. In Chapter 3 the observational results for TXS 0211-122 are presented, analyzed and discussed. The results for TXS 0828+193 are presented and analyzed in Chapter 4. The main results and final conclusions are presented in Chapter 5. Finally, in Chapter 6 an outline of future work that could be useful in the study of HzRGs is presented.

A Ω_Λ=0.73, Ω_m=0.27 and H_0=71 km s^{-1} Mpc^{-1} cosmology (Spergel et al., 2003) is adopted in this work. Using this cosmology 1″ corresponds to 8.295 kpc at z=2.34 (TXS 0211-122), and to 8.144 kpc at z=2.57 (TXS 0828+193).

Chapter 2

Observations and Data Reduction

The new observations presented here were obtained using the Optical System for Imaging and low-Intermediate-Resolution Integrated Spectroscopy (OSIRIS) on the 10.4 m Gran Telescopio Canarias (GTC).
The instrument was operated in long-slit spectroscopy mode with 100 kHz CCD readout mode. Long-slit spectra were obtained for TXS 0211-122 and TXS 0828+193 with total integration time of $\sim$ 2 hours, split into 9 integrations of $\sim$ 800 seconds for each target. A 0.41″ wide slit was used with an R1000B grism, which gave a spectral range of $\sim$ 3630 - 7500 Å. The spatial pixel scale is 0.254″ per pixel. The long slit was positioned perpendicularly to the major axis of the radio and optical emission.

A summary of the observations is presented in Table 2.1.

Object	z	Date obs. (2011)	Exp. (s)	PA (°)	Seeing (″)	FWHM (Å)	Sky transparency
(1)	(2)	(3)	(4)	(5)	(6)	(7)	(8)
TXS 0211-122	2.340	30 September	7200	22.5	0.8 - 1	3.1 - 4.0	Clear
TXS 0828+193	2.572	28 November	7380	- 45	0.8 - 0.9	6.2 - 9.4	Clear

Table 2.1: Journal of observations

Journal of observations. (1) Object name; (2) redshift; (3) date of the observations; (4) total exposure time; (5) slit position angle in degrees of North (i.e. N=0, E=90); (6) seeing; (7) full width at half maximum of the seeing disc; (8) sky transparency.

Data Reduction

The data reduction was performed using IRAF (Image Reduction and Analysis Facility) routines and the NOAO IRAF package (Tody, 1993).
The first step is to remove the instrumental signature from the data, using bias frames and flat fields. Bias frames (Figure 2.1) are obtained by taking observations with zero exposure time and with the shutter closed. They are used to determine the pixel-to-pixel variation of the offset level of the bias. Several bias frames were obtained, and were median combined, with the median image then being subtracted from all other images.

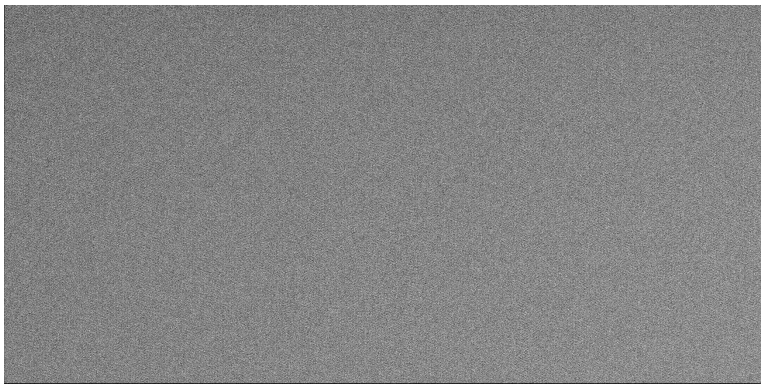

Figure 2.1: Bias image.

Flat fields (Figure 2.2) are images of uniformly illuminated surfaces and are used to determine the inter-pixel sensitivity of the instrument. Flat-fields were median combined and normalized to a mean of unity, then the target images (standard stars and objects) were divided by the normalized flat-field.

Figure 2.2: Example of a flat field image.

The wavelength calibration was performed using the IRAF tasks *identify*, *reidentify*, *fitcoords* and *transform* and using observations of HgAr (Figure 2.3) and Ne arc lamps.

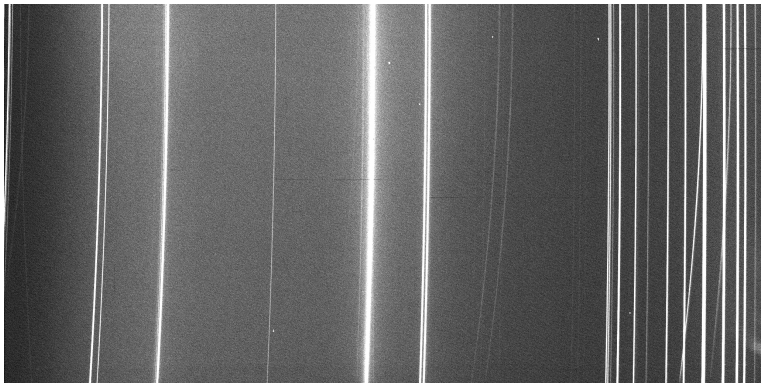

Figure 2.3: HgAr arc lamp image after removing the overscan region. The wavelength increases from left to right.

After the wavelength calibration the result has been checked measuring the wavelength of sky emission lines. For TXS 0211-122 the wavelength accuracy is $\sim$ 3 Å and for TXS 0828+193 the accuracy of the calibration is $\sim$ 0.7 Å.

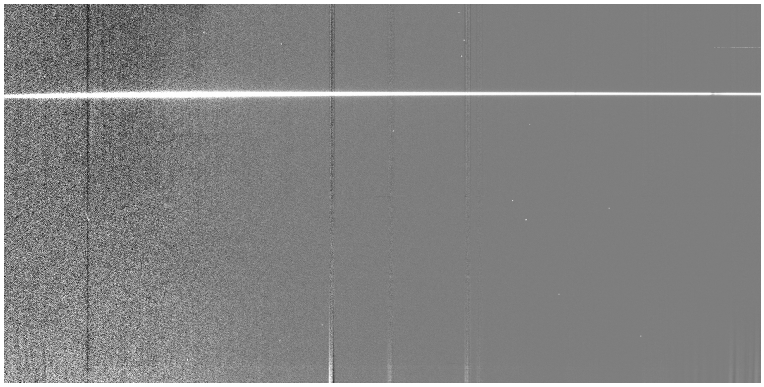

Figure 2.4: Standard star G158-100 after wavelength calibration and background subtraction.

The sky background was subtracted from the wavelength calibrated data (with IRAF *background* task). Spectra have been flux calibrated using the tasks *standard*, *sensfunc* and *calibrate*, and using observations of the spectrophotometric standard stars Grw+708247, GD99-47 and G158-100 (Figure 2.4).
The data were corrected for Galactic reddening using the task *deredden*. The final result of the calibration for one of the exposures of TXS 0211-122 can be seen in Figure 2.5.

Finally the different exposures of each galaxy were median combined, removing the cosmic ray events and improving the signal to noise ratio (S/N).
The instrumental profile was determined by measuring the FWHM of emission lines in the calibrated arc lamp spectra. The final wavelength pixel scale was 2.075 Å per pixel for TXS 0211-122 and 2.066 Å per pixel for TXS 0828+193.

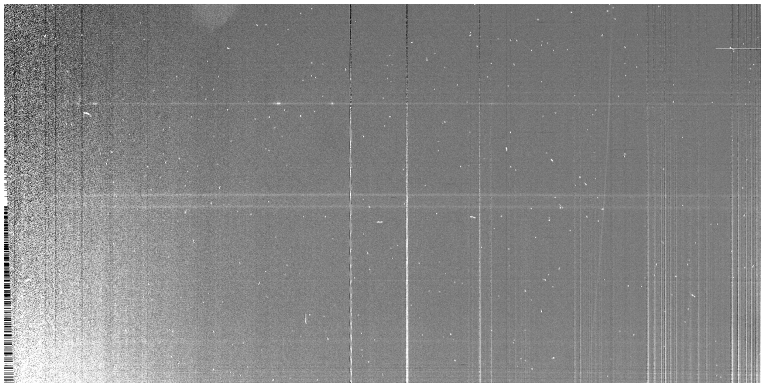

Figure 2.5: Object data after wavelength and flux calibration

Keck II data

In addition to the new observations we also made use of observations of TXS 0211-122 and TXS 0828+193 obtained using the Low Resolution Imaging Spectrometer (LRIS Oke et al., 1995) at the Keck II 10 m telescope. A 300 line mm^{-1} grating and a $1''$ wide slit were used, providing a dispersion of 2.4 Å and an effective resolution of $\sim$ 10 Å. The slit was oriented along the radio axis of the galaxy (Carilli et al., 1997). TXS 0211-122 was observed using a position angle (PA) of 104°, and TXS 0828+193 using a position angle of 44°. For observations and data reduction details see Vernet et al. (2001). Results from this data have previously been published by Vernet et al. (2001); Villar-Martín et al. (2002, 2003); Humphrey et al. (2007b,a, 2008).

The positions of the long-slits are shown in Figures 2.6 and 2.7.

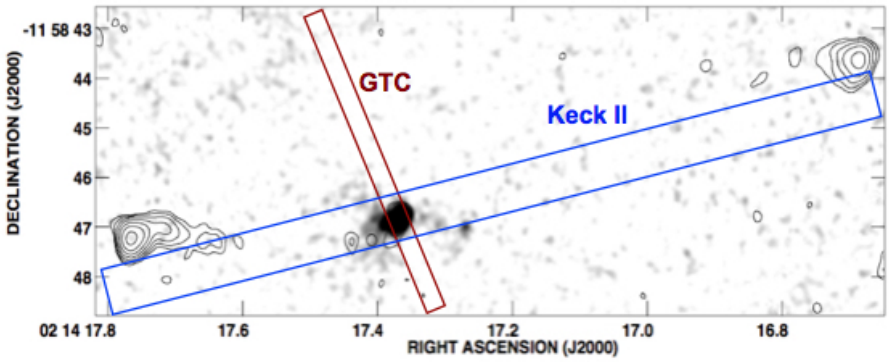

Figure 2.6: Radio image of the full field of TXS 0211-122 (Pentericci et al., 1999) with the positions of the long-slits overplotted.

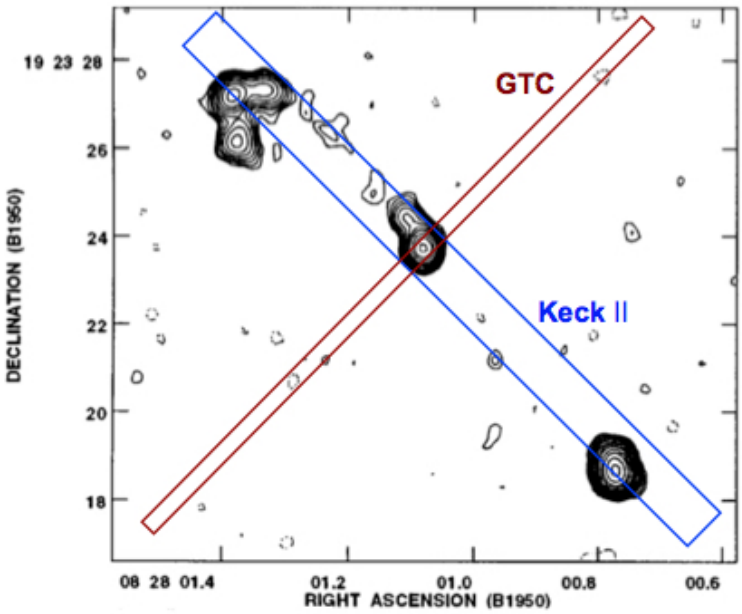

Figure 2.7: Radio image of the full field of TXS 0828+193 (Carilli et al., 1997) with the positions of the long-slits overplotted.

Chapter 3

TXS 0211-122

3.1 PREVIOUS RESULTS

TXS 0211-122 belongs to the Texas Sky Survey catalogue (Douglas et al., 1980), a catalog containing low-frequency radio sources. It was first selected as a high redshift candidate on the basis of its ultra-steep radio spectrum (USS, radio spectral index $\alpha_R \leq$ -1.30). Selecting USS radio sources has proven to be a very efficient method of finding HzRGs. This technique is based on the results of Blumenthal and Miley (1979) who found that high redshift radio sources tend to exhibit steeper radio spectra than lower redshift objects. The origin of the correlation between the steepness of the radio radio spectra and the redshift is not clear. Blundell et al. (1999) have suggested that this relationship reflects an intrinsic correlation between radio luminosity and radio spectral index. Krolik and Chen (1991) suggested that the correlation could be explained by a combination of the redshifting of a concave radio spectrum to lower radio frequencies and an increasing spectral curvature with redshift. (Klamer et al., 2006) proposed that the radio spectral index steepens with higher ambient density. At high redshift radio galaxies are likely to reside in overdense regions (e.g. McCarthy, 1993; van Ojik et al., 1996; Pentericci et al., 2000), therefore more steep-spectrum radio galaxies should be found at higher redshifts.
Optical identification and determination of the redshift of the TXS 0211-122 was performed by Röttgering (1993) confirming that it is a high redshift radio galaxy (z=2.34).

TXS 0211-122 is a powerful radio source, with a radio flux at 8.2 GHz of 24 mJy (Röttgering, 1993). It has a very large radio structure ($\sim$ 135 kpc, Carilli et al., 1997) and an optical

R-band magnitude of 22.7 (Carilli et al., 1997). The maximum stellar mass of the host of this radio galaxy is less than 1.45 $\times$ 10^{11} $M_{\odot}$ (De Breuck et al., 2010).

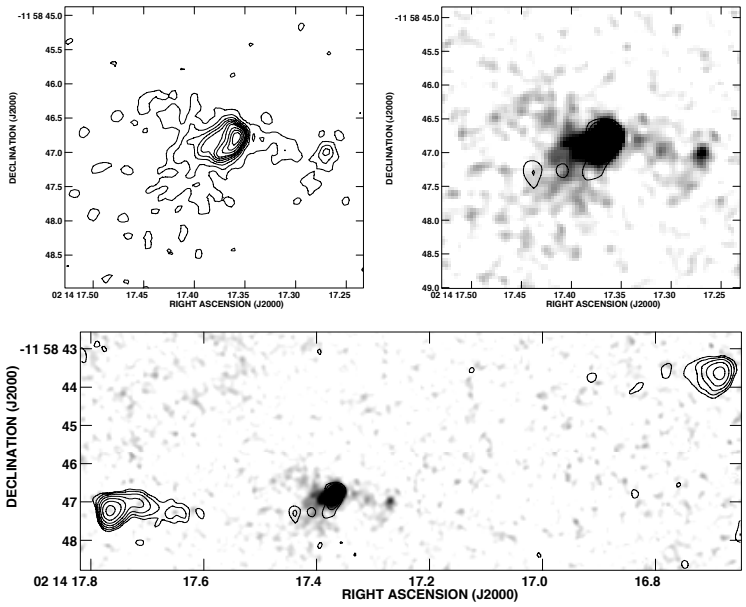

Figure 3.1: Top left: Contour representation of the UV continuum emission. Top right: Grey scale HST WFPC2 image of TXS 0211-122 overlayed on VLA (Very Large Array) radio maps. A broad-band F606W filter was used for the observations. Bottom: Radio image of the full field of TXS 0211-122. The radio frequency is 8.2 GHz. Image taken from Pentericci et al. (1999).

The radio structure consists of a bright nucleus and a smaller clump. A jet extends from the core towards the south, bends and reaches the eastern lobe (Pentericci et al., 1999). Pentericci et al. (1999) found that the UV continuum emission of this object is aligned with the axis of the radio source.

This radio galaxy is associated with an extended Lyα ($\sim$ 110 kpc), CIVλ1550 and HeIIλ1640 nebula (van Ojik et al., 1994; Villar-Martín et al., 2003), and with a $\geq$ 100 kpc scale HI absorbing structure (van Ojik et al., 1994).

van Ojik et al. (1994) found that the Lyα emission is weak when compared to higher ionization lines and that the line-emitting gas is overabundant in nitrogen. They concluded that the galaxy is undergoing a massive starburst which would produce the dust necessary to absorb the Lyα emission and that the enhancement of nitrogen could be due to photoionization or shocks.

Villar-Martín et al. (2003) detected quiet kinematics in the outer parts of the object ($\leq$ 400 km s^{-1}) and in the inner regions FWHM $\sim$ 700 km s^{-1} for all lines except Lyα (FWHM $\sim$ 1200 km s^{-1}). They detected a maximum velocity shift for the HeII line of $\sim$ 200 km s^{-1}.

Humphrey et al. (2006) found evidence for outflowing gas near the galactic nucleus. Humphrey et al. (2007b) suggest that the kinematics of the quiescent gas are consistent with infall.

This source has a high rest-frame UV continuum polarization of around 19% (Vernet et al.,

2001), and the Lyα nebula associated with this object has a polarization of 16.4$\pm$4.6% in its outer, eastern region (Humphrey et al., 2013), indicating that the nebula is partly powered by the scattering of Lyα photons by HI.
Humphrey et al. (2013) detected two continuum sources at a distance of $\sim 7''$ from the centre of the radio source. The sources were detected at the edges of the Lyα halo, one of which was found to be polarized and was also detected in Hα confirming its association with this radio galaxy. They proposed that the two continuum sources were part of a shell of gas and dust around the Lyα halo, visible because it was illuminated by the active nucleus.

3.2 GENERAL RESULTS

The emission lines Lyα, HeIIλ1640 and the doublets NVλ1440, CIVλ1550 and CIII]λ1909 are detected in all the observations. Hereinafter these lines are referred to as Lyα, HeII, NV, CIV and CIII].

The two dimensional spectra of TXS 0211-122 are shown in Figures 3.2 and 3.3. They show the spatial distribution of the brightest emission lines along the slit. The spectra are smoothed with a gaussian function with radius of 3 pixels to better show the emission line features. The zero points of the spatial scales correspond to the location of the peak of the UV continuum which is assumed to be coincident with the location of the nucleus of the galaxy. This is assumed because, as already discussed by Pentericci et al. (2001) and Villar-Martín et al. (2003) the radio core is spatially coincident with the UV continuum peak.

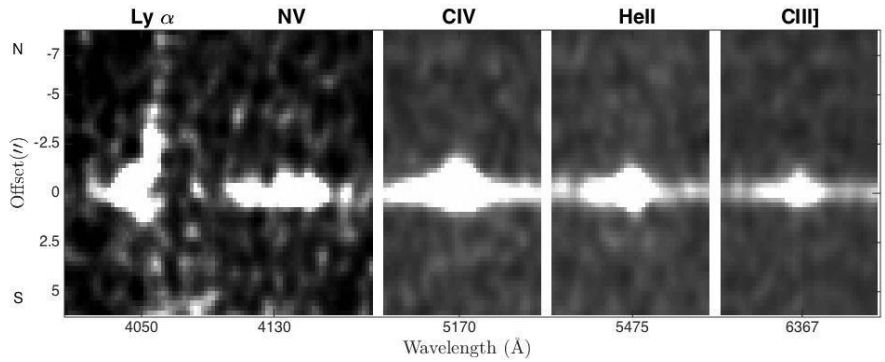

Figure 3.2: Sections of the two dimensional GTC spectrum of TXS 0211-122 obtained with the slit oriented perpendicularly to the radio axis (PA=22.5°). The zero in the spatial direction corresponds to the centre of the continuum emission. At z=2.34, 1″ corresponds to 8.295 kpc.

In the GTC spectrum (PA=22.5°) Lyα emission has a total detected extent of $\sim$ 61 kpc (7.4″). NV has a total detected extent of $\sim$ 25 kpc (3″), CIV has a total detected extent of

$\sim$ 38 kpc (4.6″), HeII has a total detected extent of $\sim$ 36 kpc (4.3″) and CIII] has a total detected extent of $\sim$ 32 kpc (3.8″). Several emission lines show spatial asymmetry. The emission lines extend further along the slit to the north than to the south.

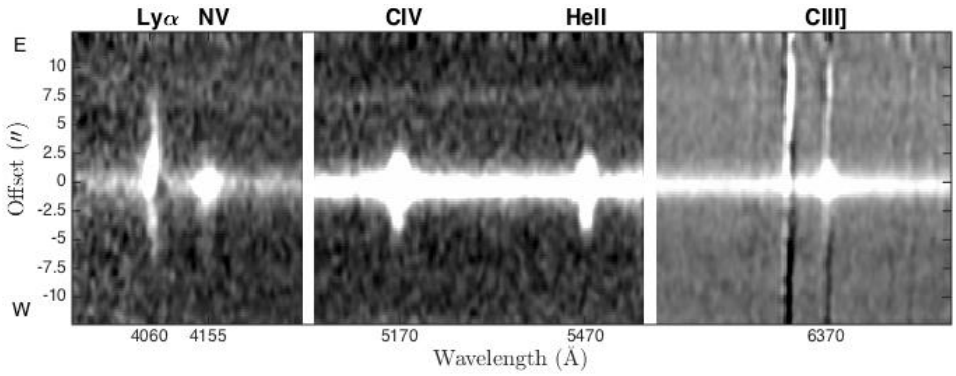

Figure 3.3: Two dimensional Keck II spectrum of the main emission lines of TXS 0211-122, with the slit oriented along the radio axis (PA=104 °). The position of the radio core (0) is identified with the brightest continuum emission.

In the direction of the radio axis (Keck II spectrum, PA=104°) the emission lines are more extended. As van Ojik et al. (1994) and Villar-Martín et al. (2003) have already shown Lyα has a total detected extent of $\sim$ 110 kpc. CIV and HeII are also extended, showing that the nebula is ionized and is significantly enriched in metals (Villar-Martín et al., 2003).

The one dimensional spectra showing different regions of TXS 0211-122 from the perpendicular slit (PA=22.5°) are shown in Figure 3.4.

Lyα emission shows clear signs of absorption. It is asymmetric, has several peaks and dips and the flux drops below the continuum level in several regions.
The CIVλ1548.2 and CIVλ1550.8 emission lines are blended creating a double peaked profile. HeII is noisy and almost not detected in the extended regions. In the central region there is evidence for an excess of flux in the blue wing of the line. This result is consistent with the results from Humphrey et al. (2006) who studied this galaxy using the Keck II data.

In the GTC spectrum (PA=22.5°) a faint continuum source is detected at 7.1″$\pm$0.1″ (59$\pm$1 kpc) from the centre of the galaxy (Figure 3.5). It is detected on the side to which Lyα is more extended. The source is unresolved, with FWHM of 0.8″$\pm$0.3″ and it has a signal to noise ratio of 4.8. Assuming that the source is associated with the radio galaxy, the rest-frame wavelength range where the source is detected is $\sim$ 1900 Å - $\sim$ 2300 Å. No emission lines are detected from this source.

The detection of this continuum source is reminiscent of an earlier result published by

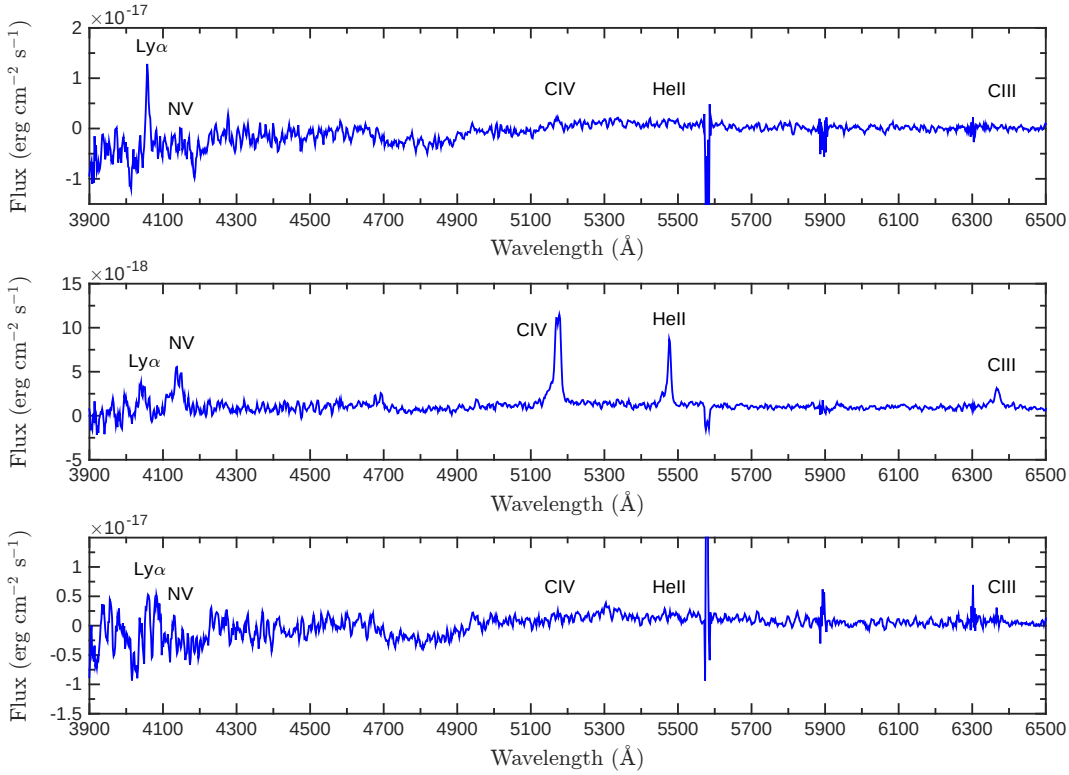

Figure 3.4: One dimensional spectra of different regions of TXS 0211-122 observed with the slit positioned perpendicularly to the radio axis. The top spectrum shows the region between -7″ and -1.3″ the middle figure shows the nuclear region (central 2″) and the bottom spectrum shows the region between 1.3″ and 7.6″. The name of each emission line is marking the position of the line. The spectra have been smoothed to reduce noise and they show some skyline residuals.

Humphrey et al. (2013) who found diametrically opposed continuum sources in the direction of the radio axis of this radio galaxy. One of their sources is clearly visible in Figure 3.3 at 7.4″ from the centre of the galaxy. The offset sources reported by Humphrey et al. (2013) were detected at the outer edge of the Lyα halo, and one showed UV continuum polarization and Hα emission close to the redshift of the radio galaxy.

Humphrey et al. (2013) interpreted their two offset continuum sources as being due to a shell of gas and dust surrounding the Lyα halo. The results found now corroborate this result. Since the source is detected in just one side of the slit in GTC data it could be an arc like feature, surrounding the Lyα emission.

Another, less probable hypothesis is that the source is a filament of gas and dust resultant from interactions between TXS 0211-122 and a companion (e.g. Ivison et al., 2008). Existing HST images are insufficiently deep to detect this faint continuum source.

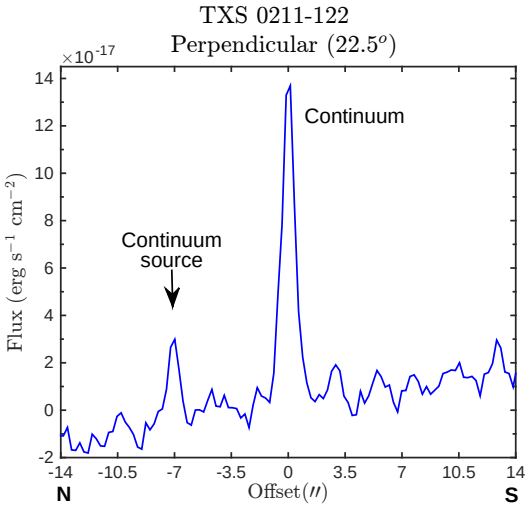

Figure 3.5: Continuum source in TXS 0211-122 observed with the slit in the direction perpendicular to the radio axis (PA=22.5°).

3.3 EMISSION LINE FLUX MEASUREMENTS AND SPATIAL PROFILES

A comparison of the spatial profiles of the Lyα line with the spatial profile of the continuum emission is shown in Figure 3.6. In order to obtain the spatial profiles two apertures were extracted. The first aperture extracted covered all the Lyα emission and the second aperture was extracted from a region close to the Lyα emission where no emission lines were detected.

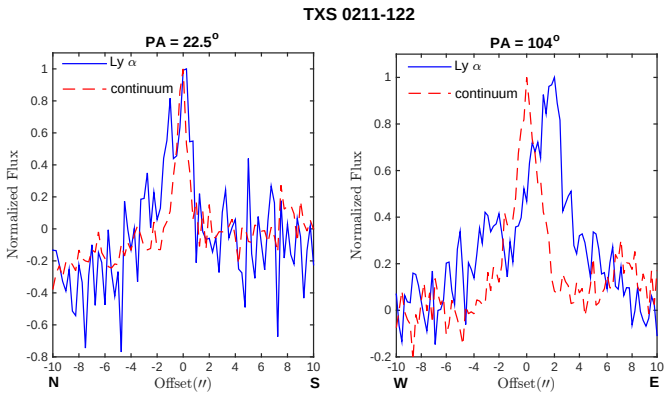

Figure 3.6: Spatial profile of Lyα compared to the continuum emission, observed with the slit positioned perpendicularly to the radio axis (left) and along the radio axis (right). The peak of Lyα emission line is offset from the peak of the continuum by $\sim 2''$ in the position of the radio axis. The fluxes are normalized in order to better show the profiles.

In TXS 0211-122 observed along the radio axis the spatial peak of Lyα emission is offset from the peak of the continuum emission by $\sim 2''$. In the direction perpendicular to the radio axis the peak of the continuum centroid and the peak of the Lyα emission are coincident. The other emission line peaks are coincident with the peak of the continuum emission (zero in the spatial direction, Figure 3.7). Resonant scattering can cause Lyα to be spatially shifted from the high ionization lines (Röttgering et al., 1997), and this seems likely to be the case of the spatial shift of Lyα. The fact that we only see a shift in the direction of the radio axis may be due to an offset between the nucleus and the maximum Lyα optical depth (or maximum HI column density) along the radio axis.

IRAF routines were used to measure the emission-line fluxes from simple line integrals. Flux uncertainties were estimated based on the fitting uncertainties and the uncertainties in the continuum level. The errors associated with the observed emission fluxes have been calculated using the expression

$$\sigma = N\,\Delta\,\frac{std_{cont}}{\sqrt{N}}\,, \tag{3.1}$$

where *N* is the number of pixels used in the measurement of the line flux, std_{cont} is the standard deviation of the continuum emission measured close to the emission line, Δ is the wavelength dispersion in Å per pixel. They represent the 1σ confidence interval, fluxes below 3σ were discarded. Zero is the location of the peak of the continuum light from the galaxy.

The surface brightness profiles of the observed emission lines of TXS 0211-122 are shown in Figure 3.7.

For TXS 0211-122 observed along the radio axis we see that the Lyα emission spatial profile is quite different to the spatial profile seen in the direction perpendicular to the radio axis. In the direction of the radio axis (PA=104°) Lyα peaks at $\sim 2''$. In GTC data (PA=22.5°) the peak is at the spatial zero.

Lyα emission is unusually faint when compared to the other UV lines. van Ojik et al. (1994, 1997) attributed this to very strong absorption of Lyα by dust mixed through the emission line gas.

To check if resonant scattering is responsible for the extended Lyα in the direction perpendicular to the radio axis, one aperture was extracted covering the most extended Lyα emission (-5.1″ to -3″, see Figure 3.8) where HeII is undetected.

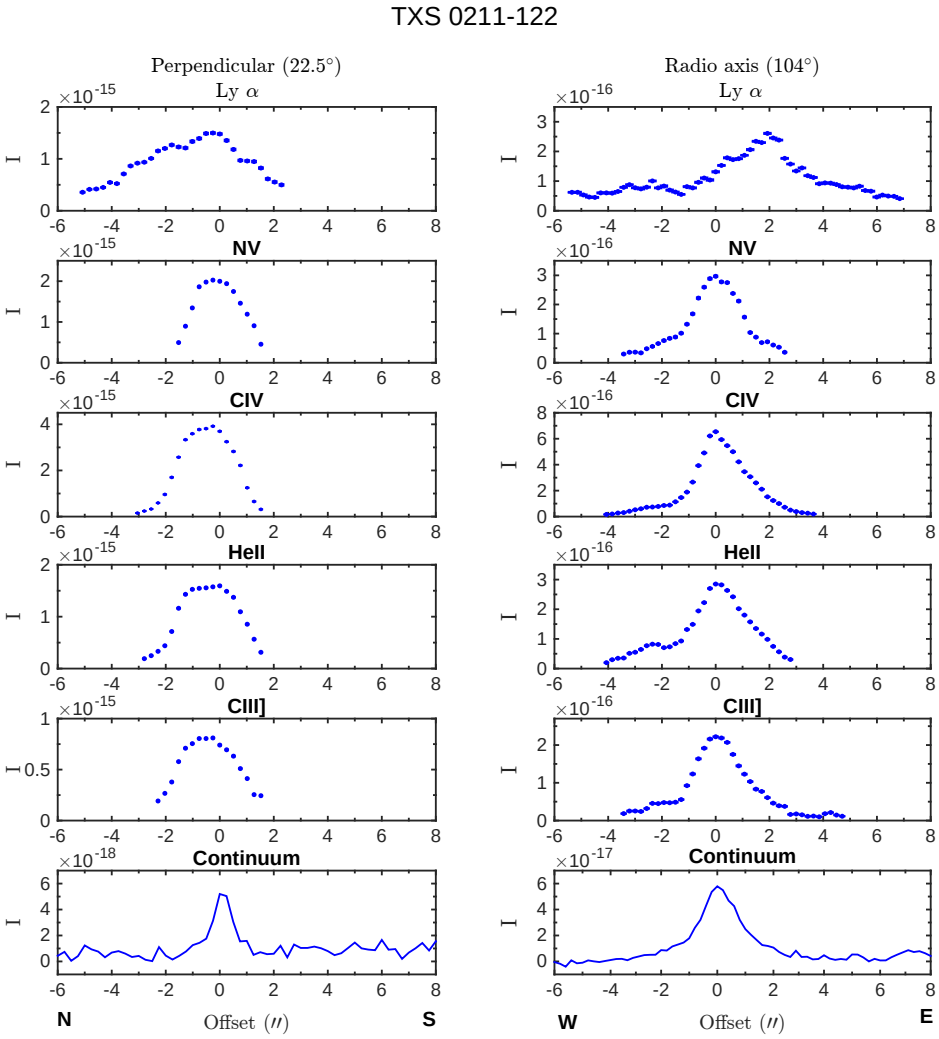

Figure 3.7: Surface brightness (I) of the different emission lines and continuum profile (bottom figures) in TXS 0211-122. The left figures are the surface brightness values observed perpendicularly to the radio axis and the right figures the surface brightness values observed along the radio axis. The flux units are erg cm^{-2} s^{-1} arcsec^{-2}. Zero in the spatial direction represents the peak of the continuum emission.

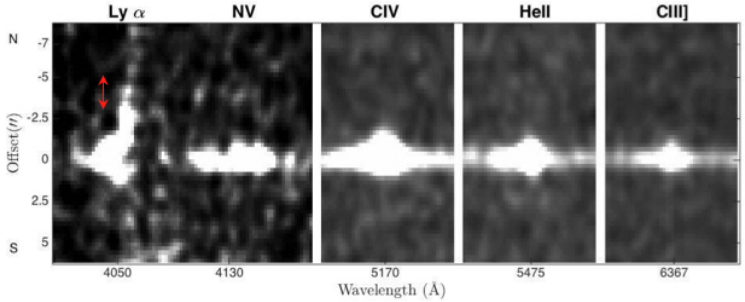

Figure 3.8: Sections of the two dimensional GTC spectrum of TXS 0211-122 obtained with the slit oriented perpendicularly to the radio axis (PA=22.5°). The red arrow indicates the region between -5.1″ and -3″, where an aperture was extracted.

Estimating the flux that HeII would have at the 3σ level the ratio Lyα/HeII was calculated, and a lower limit of $\geq$2.8 was obtained. Typically the Lyα/HeII ratio has a value of $\sim$ 11.7 (Humphrey et al., 2008). Since this result is a lower limit, the extended Lyα emission could be due to resonant scattering of Lyα photons. However, the lower limit is also consistent with photoionization (AGN or stars) and ionization by shocks.

3.4 LINE RATIOS AND COMPARISON WITH MODELS

In this section we show how the ratios of the different emission lines vary along the slits and use line ratio diagnostic diagrams to examine the conditions and properties of the emission line regions.

One way of determining the ionization mechanism of the gas is to compare the observed line ratios to model predictions. In this section a comparison is made between the results of our observations and photoionization and shock models. Both photoionization and shock models were used because photoionization models are able to reproduce the results in most HzRGs (Fosbury et al., 1982; Villar-Martín et al., 2002, 2003) but in some radio galaxies shocks seem to contribute significantly to the ionization of the gas (e.g. Villar-Martín et al., 1999b; Tadhunter et al., 2000).

The photoionization model runs were performed by A. Humphrey, who computed photoionization models using the multipurpose code MAPPINGS 1e (Binette et al., 1985; Ferruit et al., 1997), as part of a separate project (Humphrey et al., in preparation). The model has several parameters, gas density of hydrogen (n_H), ionization parameter (U), α_i and gas metallicity (Z).

The ionization parameter is defined as

$$U = \frac{Q}{4\pi r^2 n_H c}\,, \tag{3.2}$$

where Q is the ionizing photon luminosity, r is the distance of the ionized cloud from the ionizing source, c is the speed of light, and n_H is the hydrogen gas density. It indicates how intense the ionizing radiation is as felt by the cloud. In the grid of photoionization calculations, U increases from 0.00005 to 0.00005$\times$ 3^9 in multiplicative steps of times 3.

α_i is the spectral index of the ionizing continuum. The ionizing continuum has the form

defined by

$$f_\nu \propto \nu^{\alpha_i}\,, \tag{3.3}$$

where ν is the frequency. Finally, the metallicity takes the values Z=0.2 $Z_\odot$, Z=$Z_\odot$ and Z=3 $Z_\odot$, where $Z_\odot$ is the solar metallicity (Asplund et al., 2006).
The chemical abundances have been scaled with all metals scaled proportionally to oxygen, except nitrogen, which is scaled quadratically with oxygen (Henry et al., 2000).

Photoionization by a power law of index -1.0 was used because according to the results of Villar-Martín et al. (1997) it is best able to reproduce the ratios observed in HzRGs. For the hydrogen density, a value of n_H=100 cm^{-3} was chosen because previous studies have found, by various lines of argument, that the extended emission line gas has very approximately this density (McCarthy et al., 1990; Villar-Martín et al., 2002, 2003).
Besides photoionization by the AGN, ionizing shocks may also play a role in heating the gas, therefore shock and shock plus precursor models computed by Allen et al. (2008) are also considered. These models have solar metallicities, n_H=100 cm^{-3}, the shock velocities are in the range 100 km $s^{-1} \leq$ v $\leq$ 1000 km s^{-1}, the magnetic field B=32.3 μ G, and the magnetic parameter B/$n^{1/2}$=3.23 μ G $cm^{3/2}$, where n is the pre-shock number density.

The emission lines from different elements are expected to be sensitive to several parameters (gas temperature, density, metallicity, ionization parameter), therefore ratios between emission line intensities can provide information about the chemical abundances, the physical conditions and the ionizing mechanism of the ionized gas (Baldwin et al., 1981; Robinson et al., 1987).

Lyα, NV, CIV, HeII and CIII] are helpful to distinguish between ionization mechanisms and can provide information on the abundance of these elements De Breuck et al. (2000).
Lyα, CIV and NV are resonance lines and therefore can depend on the geometry of the gas and its dust content (Villar-Martín et al., 2006).
The ratio CIV/CIII] depends strongly on the ionization parameter, but also has some dependence on the metallicity due to a temperature effect (Villar-Martín et al., 1997, 2001).
The ratio NV/CIV is rather insensitive to variations in density and is widely regarded as a good metallicity indicator (e.g. Hamann and Ferland, 1993; Groves et al., 2004). This is because secondary production of nitrogen is thought to give rise to quadratic behaviour of the nitrogen abundance as a function of oxygen abundance, and overall metallicity (N/H $\propto$ $(O/H)^2$, Henry et al., 2000).
The problem with this line ratio is that NV and CIV have different ionization potentials (N^{4+} ions have an ionization potential of 77.4 eV, C^{3+} ions have an ionization potential of 47.9

eV), and different excitation energies therefore they do not depend only on metallicity.
HeII is a non-resonant recombination line and is relatively insensitive to a wide variety of physical conditions, e.g., ionization parameter and metallicity, giving us a useful baseline by which to examine the fluxes of other emission lines.
The behaviour of the emission lines described above was deduced from an inspection of photoionization model grids.

In order to better understand the differences in the emission line ratios along the slit, one dimensional spectra were extracted (using the task *blkavg* in IRAF) from several apertures for comparison against ionization models. The central aperture contains almost all the continuum emission, the other ones were chosen to examine the variations between the different regions of the nebula. Table 3.1 and table 3.2 show line ratios for GTC and Keck II data, respectively. These are the values used in the line ratio diagrams.

Pos. (1)	Lyα/HeII (2)	Lyα/CIV (3)	Lyα/NV (4)	CIV/HeII (5)	CIV/CIII] (6)	NV/HeII (7)	NV/CIV (8)
-3.3″: -1.8″	5.0±0.3	-	-	-	-	-	-
-1.8″: -0.8″	2.9±0.2	1.5±0.2	-	2±0.2	3.1±0.2	-	-
-0.8″: 0.8″	0.8±0.1	0.34±0.1	0.5±0.1	2.36±0.06	4.51±0.08	1.56±0.09	0.66±0.08
0.8″: 1.8″	2.5±0.3	1.6±0.3	-	1.5±0.3	1.9±0.3	-	-

Table 3.1: Emission line ratios from several apertures in the TXS 0211-122 spectrum observed in the direction perpendicular to the radio axis (PA=22.5°). Columns are as follows: (1) position of the aperture along the slit in arcseconds; (2) the Lyα/HeII ratio; (3) the Lyα/CIV ratio; (4) the Lyα/NV ratio; (5) the CIV/HeII ratio; (6) the CIV/CIII] ratio; (7) the NV/HeII ratio; (8) the NV/CIV ratio.

The nuclear aperture shows a difference in line ratios between the Keck II data and GTC data but this could be due to a slight misalignment between the slits and/or to the different apertures chosen in each case.

Pos. (1)	Lyα/HeII (2)	Lyα/CIV (3)	Lyα/NV (4)	CIV/HeII (5)	CIV/CIII] (6)	NV/HeII (7)	NV/CIV (8)
-5.8″ : -3.9″	5.4±0.3	3.6±0.3	-	1.5±0.4	1.7±0.4	-	-
-3.9″ : -1.9″	1.3±0.1	1.4±0.1	1.4±0.1	1.0±0.1	3.3±0.2	0.9±0.2	1.0±0.2
-1.9″ : 1.3″	0.65±0.05	0.33±0.04	0.67±0.04	1.94±0.03	3.43±0.05	0.96±0.05	0.49± 0.04
1.3″ : 4.1″	4.4±0.1	2.52±0.07	4.58±0.09	1.8±0.1	2.8±0.12	1.0±0.2	0.5± 0.2

Table 3.2: Emission line ratio measurements from the TXS 0211-122 spectrum, observed along the radio axis (PA=104°). Columns are as in 3.1.

Figure 3.9 shows how the different line ratios vary along the slits.

The UV emission line ratios of this radio galaxy show unusually weak Lyα relative to

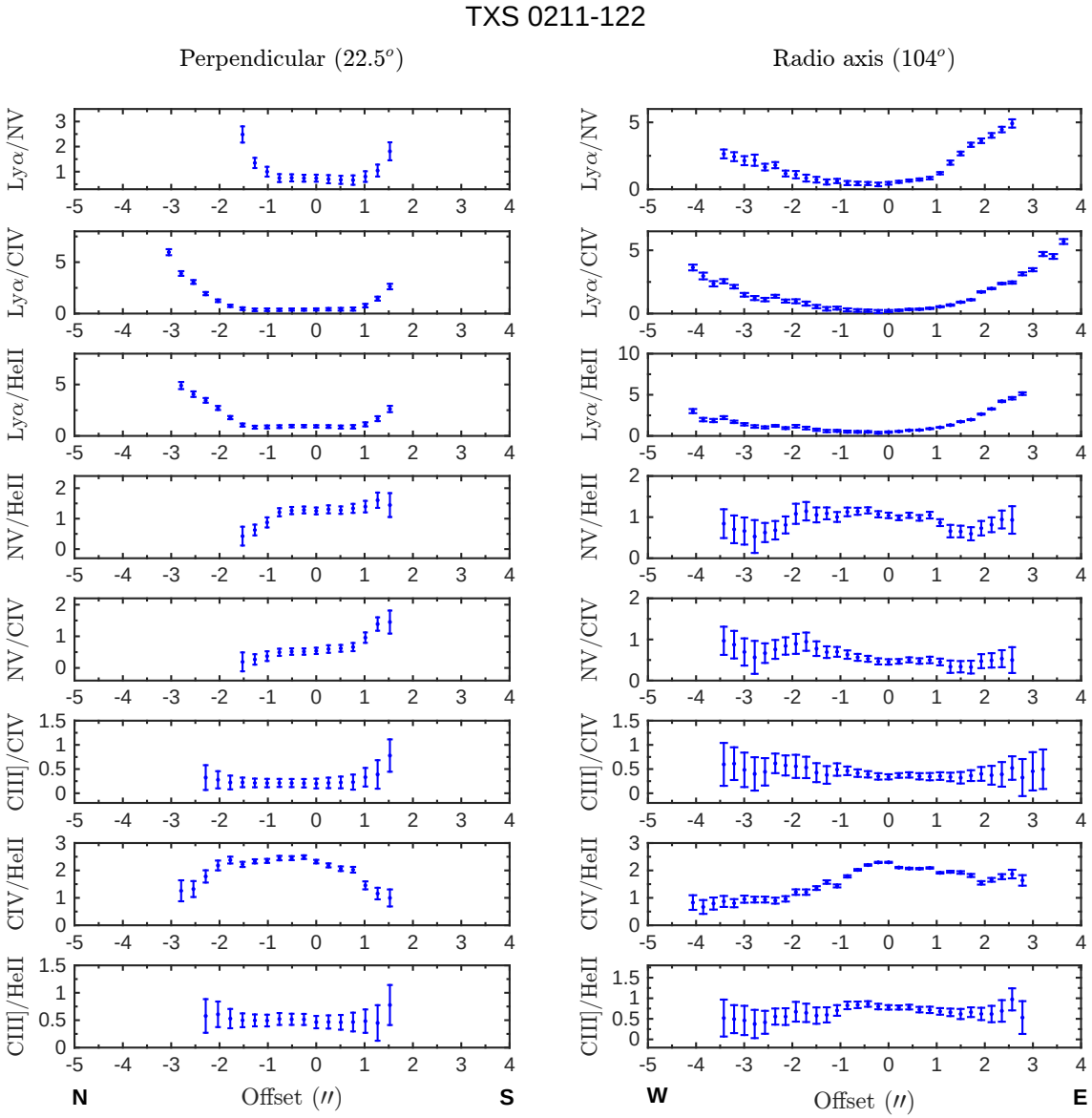

Figure 3.9: Ratios between the emission lines of TXS 0211-122 as a function of distance in the galaxy. In the left we have the flux ratios in the direction perpendicular to the radio axis (PA=22.5°) and in the right in the direction of the radio axis (PA=104°).

the other lines and strong NV compared to those of CIV, HeII and CIII] (Humphrey et al., 2008). The ratio between Lyα and the other emission lines presents a "U shape" along both slits. This provides evidence for a variation in Lyα absorption, with strong absorption in the central regions, with progressively less absorption at larger radii. However, the Lyα/HeII ratio remains well below the AGN-photoionization value of $\sim$12 obtained from the MAPPINGS model grid.

If, as suggested by van Ojik et al. (1994) the Lyα emission is being depressed by dust then CIV may also show signs of having been absorbed because it is also a resonant line

and thus may also suffer from dust absorption. However, if CIV was being absorbed, the line ratio CIV/HeII should show a similar U-shaped profile of Lyα/HeII but this is not present. Moreover, if CIV was absorbed the ratio CIV/HeII would probably show lower values than typical HzRGs ($\sim$ 1.75, Humphrey et al., 2008). This suggests that the impact of absorption on CIV is small.

Line ratios between the different emission lines are now compared to the ionization models. Diagnostic diagrams were constructed in order to visualize the comparison (Baldwin et al., 1981).

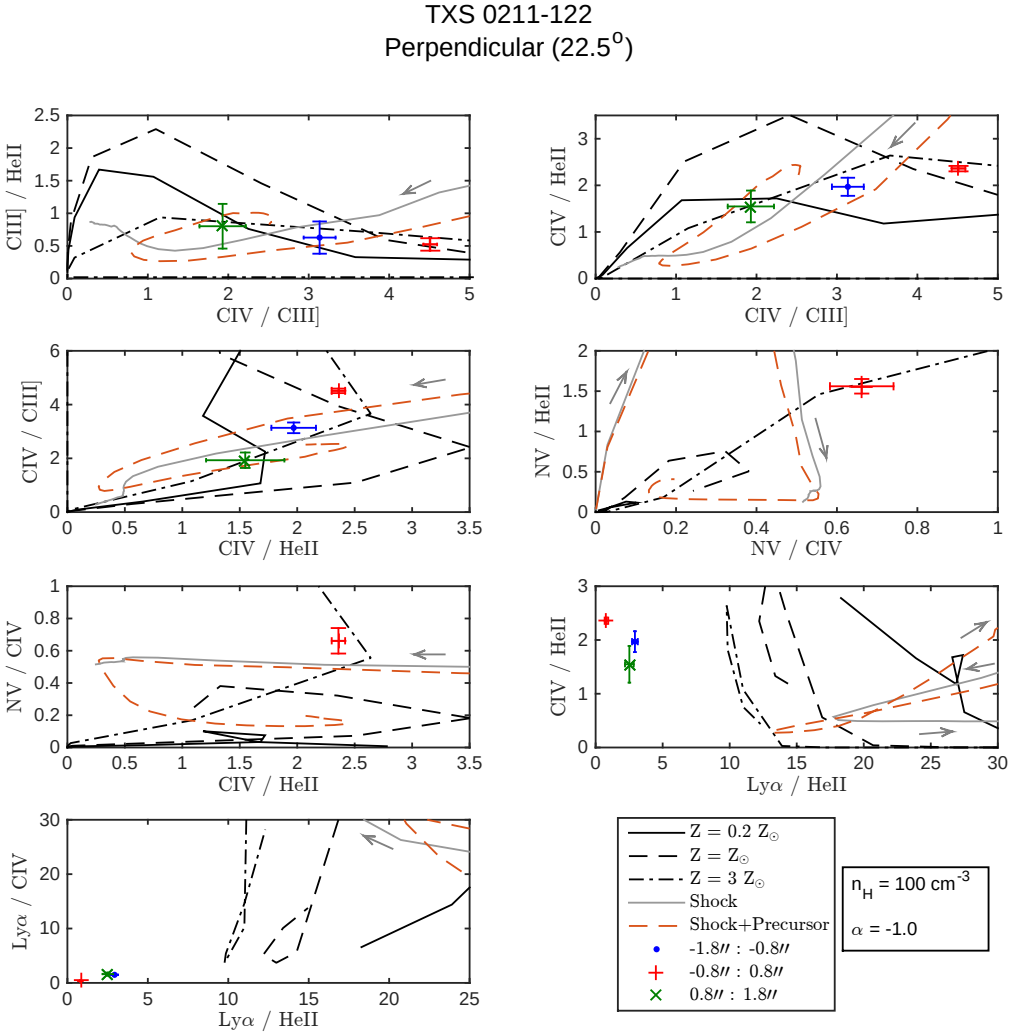

Figure 3.10: Model grids computed using the code MAPPINGS plotted on several diagrams. The flux ratios of TXS 0211-122 observed with the slit in the position perpendicular to the radio axis plotted on diagnostic diagrams involving Lyα, NV, CIV, HeII and CIII]. The shock models by Allen et al. (2008) are also shown. Grey solid lines denote the predictions of pure shock models, and orange-dotted lines denote the prediction of shock plus precursor models. The parameters are the same for all figures. The arrows indicate the direction of increasing shock velocity.

The emission line flux ratios of NV/CIV and NV/HeII are usually used to infer metallicities (Villar-Martín et al., 1999a; Fosbury et al., 1999; De Breuck et al., 2000; Vernet et al., 2001). However, in the case of the observation with the slit in the direction perpendicular to the radio axis NV is only detected in one aperture thus diagrams consisting of CIV/HeII and CIII]/CIV ratios will be used (as proposed by Nagao et al., 2006).
The problem with using only CIV, CIII] and HeII is that they depend on several parameters, not only on the metallicity. Besides, for each value of the ratios two possible metallicities exist, meaning that there is a strong degeneracy.

According to the diagnostic diagrams CIII]/HeII versus CIV/CIII], CIV/HeII versus CIV/CIII] and CIV/CIII] versus CIV/HeII in Figure 3.10 a photoionization model with Z=3$Z_{\odot}$ and a change in ionization parameter is able to reproduce our flux ratio measurements. However, the region from 0.8″ to 1.8″ can be reproduced by a photoionization model with Z=3$Z_{\odot}$ or by a photoionization model with Z=0.2$Z_{\odot}$. This illustrates the degeneracy between metallicity solutions when using the CIV, HeII and CIII] line ratios.
In the direction perpendicular to the radio axis NV is only detected in the centre of the galaxy. The ratio NV/HeII versus NV/CIV suggests a metallicity of Z=3$Z_{\odot}$.
The NV strength in relation to CIV and HeII suggests high levels of chemical enrichment of the gas. The small variation in CIII]/HeII suggests a small variation in C/He (and thus C/H and, perhaps, O/H).
It seems that an AGN photoionization model reproduces well our results, however we must be cautious, seeing effects and our lack of information about the morphology of the gas could potentially contaminate some off-nuclear regions of the perpendicular slit with emission from the AGN ionization cones.

The results for the observations with the slit in the direction of the radio axis (PA=104°) are shown in Figure 3.11.

In aperture -5.8″ to -3.9″ the degeneracy due to the use of CIV, HeII and CIII] line ratios is clearly visible. The line ratios observed in aperture -3.9″ to -1.9″ lie far from the models in most of the diagrams.
Most diagrams show that AGN photoionization, shock and shock plus precursor models reproduce equally well most of the line ratios observed.

None of the models reproduce the Lyα/HeII and Lyα/CIV line ratios. Photoionization models, shock and shock plus precursor models all predict higher Lyα/HeII ratios than those measured. Lyα is always too faint relative to the other UV lines, by a factor of $\sim$ 7. The

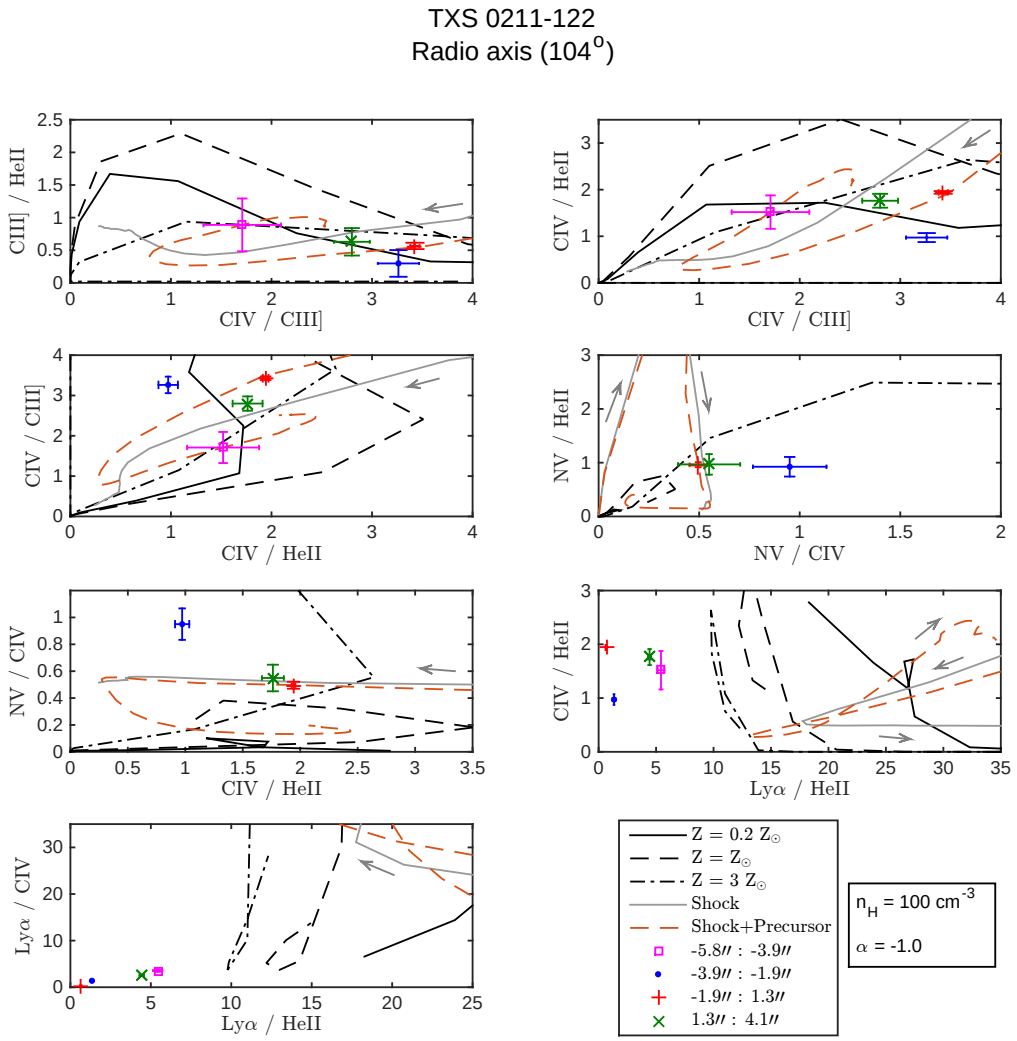

Figure 3.11: Flux ratios of TXS 0211-122 observed with the slit along the radio axis plotted on diagnostic diagrams involving Lyα, NV, CIV, HeII and CIII]. MAPPINGS photoionization models are shown. The shock models by Allen et al. (2008) are also shown. Grey solid lines denote the predictions of pure shock models, and orange-dotted lines denote the prediction of shock plus precursor models. The parameters are the same for all figures. The arrows indicate the direction of increasing shock velocity.

cause of this discrepancy is likely to be strong absorption of Lyα by HI (and possibly dust).

The diagnostic diagrams suggest high metallicities, even in regions far from the nucleus. These results are in agreement with the results from Vernet et al. (2001) who found that the metallicities of the extended emission line regions of powerful HzRGs are close to solar or supersolar values. At z=2.34 this galaxy has (probably) already undergone an intense period of star formation and thus chemical enrichment.

In this section we compared the observed line ratios to model predictions. However, due

to the low number of parameters considered here, conclusions from the comparison with models should be considered indicative but not exhaustive. In order to determine more accurate gas chemical abundances more detailed modelling will be required.

3.5 KINEMATICS

Kinematic information was extracted from the two dimensional spectra by fitting single Gaussians to the spatial profiles of the emission lines. Gaussians were fitted at each spatial position along the emission line, summing (in space) a number of pixels to increase S/N. In this galaxy the Lyα velocity profile deviates from a Gaussian due (presumably) to HI absorption which may have modified significantly the kinematics from the intrinsic kinematics of the line. The systemic velocity was determined from the peak of HeII emission in the centre of the galaxy (peak of the UV continuum emission).

The gas velocity was calculated using the formula

$$v = c\,\frac{\lambda - \lambda_0}{\lambda_0}\,, \tag{3.4}$$

where c is the speed of light, λ is the observed wavelength and λ_0 refers to the wavelength measured at the centre of the galaxy, determined from the HeII emission line.
The uncertainty in the velocity is estimated to be $(\sqrt{2}FWHM)/(2.35S/N)$, where S/N is the signal to noise ratio of the observed emission line. The FWHM values have been corrected in quadrature for the instrumental broadening

$$FWHM_{corr} = \sqrt{FWHM^2_{measured} - FWHM^2_{instrument}} \quad [\text{Å}]\,. \tag{3.5}$$

Figure 3.12 shows the overall velocity centroids of Lyα, HeII and CIV emission along TXS 0211-122. The lines show strong spatial variation in their velocity centroids.

The maximum difference of Lyα emission line velocity and the systemic velocity of the galaxy observed perpendicularly to the radio axis (PA=22.5°) is $\sim$ 1200 km s^{-1}. The maximum velocity shift of HeII across the nebula is $\sim$ 240 km s^{-1} and the maximum velocity shift of CIV is $\sim$ 230 km s^{-1}. In the direction perpendicular to the radio axis HeII and CIV show similar velocity curves to each other, but both differ significantly from the velocity curve of Lyα, suggesting that the measured kinematics of Lyα emission are strongly affected by HI absorption or scattering.

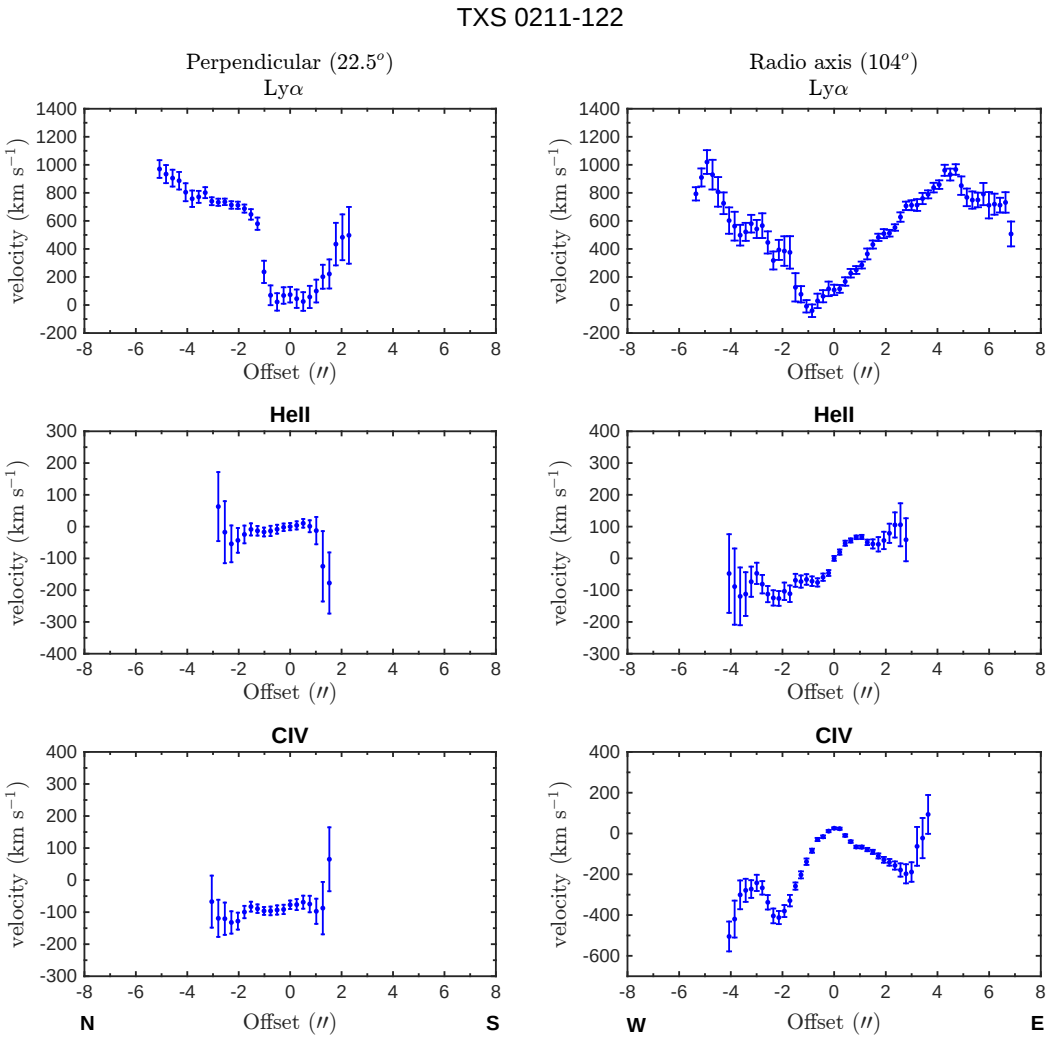

Figure 3.12: Lyα (top), HeII (middle) and CIV (bottom) velocity profiles. The figures in the left represent the variation in the direction perpendicular to the radio axis, while the figures in the right represent the variation along the radio axis.

In the direction of the radio axis (PA=104°) the maximum difference between Lyα velocity and the systemic velocity is $\sim$ 1000 km s^{-1}. HeII shows a maximum velocity shift of $\sim$ 230 km s^{-1} and CIV has a maximum velocity shift of $\sim$ 600 km s^{-1}. In this direction HeII shows a rather constant velocity curve. The velocity curve of Lyα shows a large range in velocity. Once again this could be due to HI absorption or scattering. The velocity curve of CIV also differs from the velocity curve of HeII. CIV seems to be blueshifted relative to HeII. This result is further explored later in this section.

Figure 3.13 shows how the FWHM Lyα, HeII and CIV vary along the two slits.

Following Villar-Martín et al. (2002) quiescent emission refers to gas with FWHM $\leq$ 1000

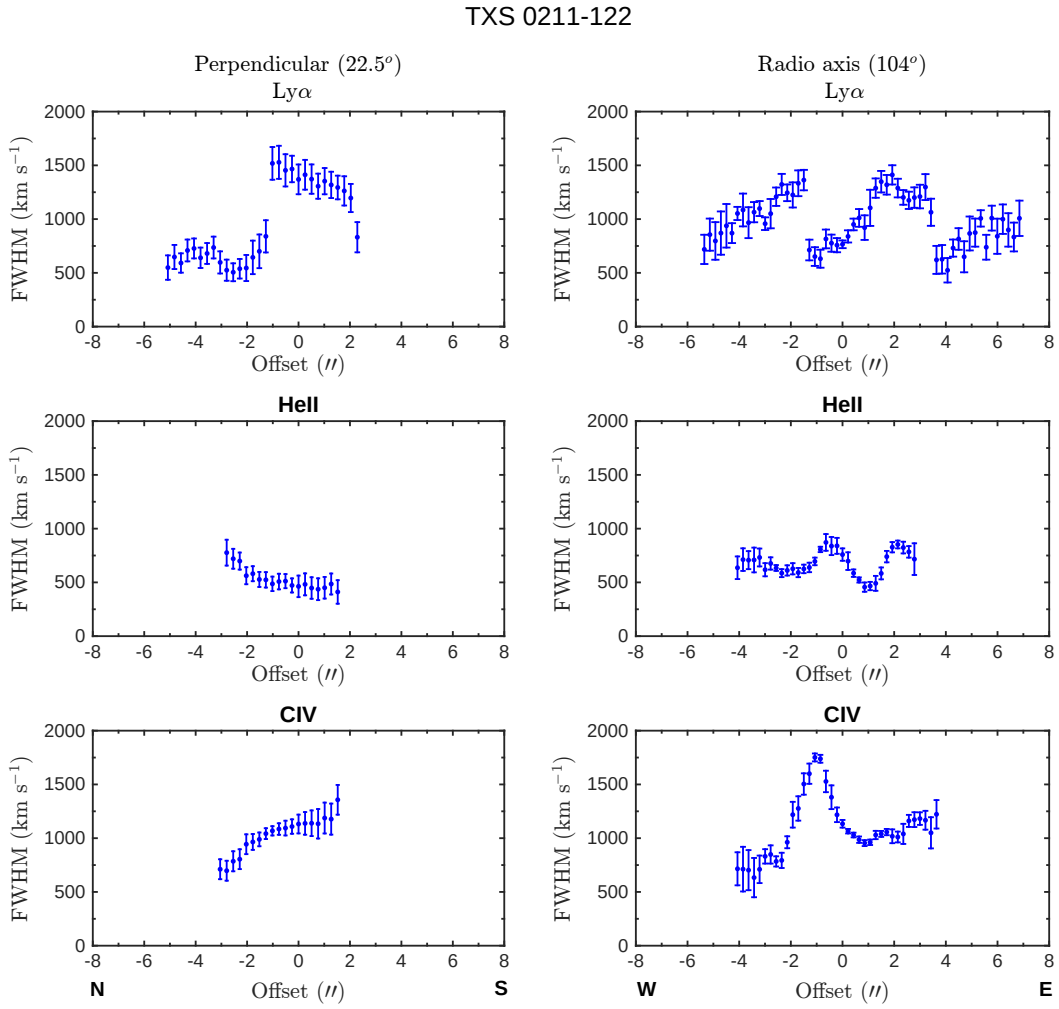

Figure 3.13: FWHM of Lyα, HeII and CIV. The figures in the left represent the variation in the direction perpendicular to the radio axis, while the figures in the right represent the variation along the radio axis.

km s^{-1} and perturbed emission refers to emission lines with FWHM $\geq$ 1000 km s^{-1}.

In the direction perpendicular to the radio axis there is a sudden jump in the FWHM and velocity curve of Lyα at -1.27″. This jump is not seen in the other UV lines, suggesting a change in the impact of absorption or resonant scattering on Lyα.

In the direction of the radio axis (PA=104°) Lyα shows several changes in the FWHM. Villar-Martín et al. (2003) found narrow and broad component in the Lyα emission of this radio source. The differences in the FHWM(Lyα) observed in Figure 3.13 may be due to the different components. In regions where the broad component is affecting more the width of the line broad lines are produced, and in regions where the narrow component dominates

the FWHMs are lower.

As previously reported by Villar-Martín et al. (2003) the HeII velocity curve displays quiescent kinematics (FWHM $\sim$ 700 km s^{-1}) in the direction of the radio axis. In the direction perpendicular to them HeII also shows quiescent kinematics.
The radial velocity (< 200 km s^{-1}) and FWHM (< 850 km s^{-1}) of HeII in both regions of the galaxy suggest that the gas dynamics is dominated by gravitational motions.
The detection of different line velocity widths for CIV and HeII may indicate that the lines are produced in regions with different physical conditions. However, the different FWHMs could also be due to the fact that CIV is a doublet, and thus naturally broader than HeII.

Looking at the results obtained for the Keck II data (PA=104°) and comparing the plot of CIV/HeII (Figure 3.9) and the velocity of CIV (Figure 3.12) it can be seen that the lowest values of CIV/HeII have the highest blueshift. This result is consistent with the presence of ionized gas outflows along the radio axis, with a relatively lower ionization state, as have been found in a number of powerful radio galaxies at low to high redshifts (e.g. Villar-Martín et al., 1999b; Humphrey et al., 2006).
In order to investigate possible correlations between the CIV/HeII ratio and the velocities of the different emission lines the Spearman (1904) rank correlation coefficient was calculated.

The results are presented in Figure 3.14. ρ is the Spearman's rank correlation coefficient. This figure shows a strong positive correlation (ρ=0.932) between CIV's velocity and the ratio CIV/HeII in the direction of the radio axis. That is, the higher the redshift, the higher the ratio. It also shows a positive correlation (ρ=0.620) between HeII's velocity and CIV/HeII. In order to test if the values of 0.932 and 0.620 are significant they were compared to critical values for Spearman's rank correlation coefficient. Both correlations are significant at a confidence level of more than 99%.
In the direction perpendicular to the radio axis no correlation is apparent, suggesting that the ionized outflowing gas is preferentially situated along the radio axis.

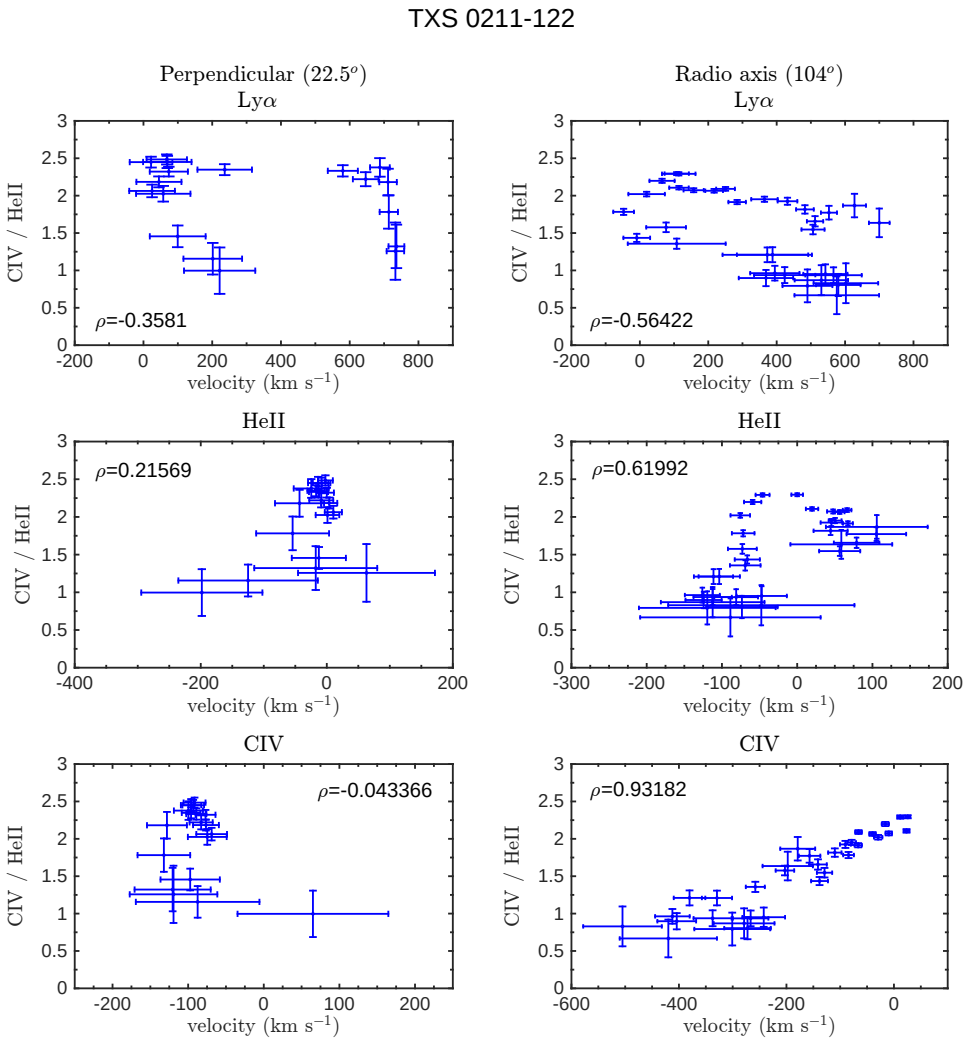

Figure 3.14: Variation of CIV/HeII ratio with the velocity of different emission lines. The top left panel shows the ratio CIV/HeII as a function of the velocity of Lyα in the perpendicular slit, the top right panel shows the variation of CIV/HeII as a function of the velocity of Lyα along the radio axis, the middle left panel shows the variation of CIV/HeII as a function of the velocity of HeII in the perpendicular slit, the middle right panel shows the variation of CIV/HeII as a function of the velocity of HeII in the slit placed along the radio axis, the bottom left figure shows how the CIV/HeII varies with the velocity of CIV in the perpendicular slit and the bottom right figure shows how the CIV/HeII varies with the velocity of CIV along the radio axis. ρ represents the Spearman's rank correlation coefficient.

Chapter 4

TXS 0828+193

4.1 PREVIOUS RESULTS

TXS 0828+193 belongs to the Texas Sky Survey catalogue (Douglas et al., 1980). Just like TXS 0211-122, TXS 0828+193 was also selected as a high redshift candidate on the basis of its USS and later confirmed as a high redshift radio galaxy by Röttgering (1993) .

TXS 0828+193 has a large radio source (98 kpc, Carilli et al., 1997), with a total radio flux at 4.7 GHz of 22 mJy. It is found at z=2.57 (van Ojik, 1995) and has an R-band magnitude of 20.7 (Carilli et al., 1997).
The radio structure consists of several clumps (Pentericci et al., 1999) that can be seen in the left panel of Fig. 4.1, and has a double morphology (Röttgering et al., 1994) with a jet extending from the core to the northern hotspot (Fig. 4.2). The UV continuum is elongated and aligned with the axis of the radio source Pentericci et al. (1999).
The host galaxy has a maximum stellar mass of $< 3.98 \times 10^{11}$ $M_{\odot}$ (Seymour et al., 2007). van Ojik et al. (1997) found that the blue wing of the Lyα emission profile is absorbed by neutral gas. CO(3-2) emission was found in the halo of the radio structure by Nesvadba et al. (2009). This source has an intermediate continuum polarization of around 10% (Vernet et al., 2001).
Villar-Martín et al. (2002) discovered a giant halo of quiescent gas extending beyond the radio structures ($\sim$ 130 kpc, in our cosmology). They also detected two kinematic components in Lyα, CIV and HeII. A kinematically quiescent component (FWHM < 400 km s^{-1}) extending across the whole object and beyond the radio structures, and a kinematically disturbed

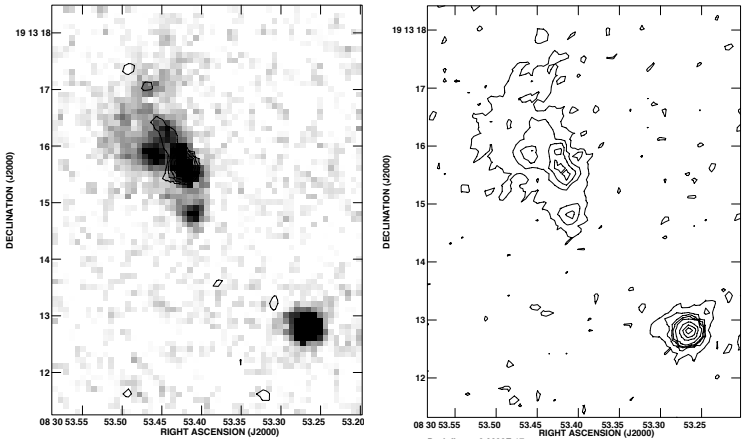

Figure 4.1: Left: Grey scale HST WFPC2 image of TXS 0828+193 overlayed on VLA (Very Large Array) radio maps. The filter used for the observations was a broad-band F675W filter. Right: Contour representation of the UV continuum emission. Image taken from Pentericci et al. (1999).

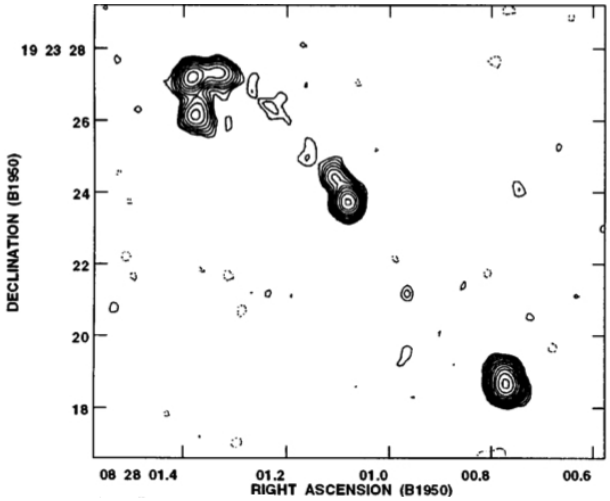

Figure 4.2: Image of the full field of TXS 0828+193. The radio frequency is 4.7 GHz. Image taken from Carilli et al. (1997).

component (FWHM $\sim$ 1200 km s^{-1}) inside the radio structure. Humphrey et al. (2006) found that the perturbed component is blueshifted in relation to the quiescent component, and that the disturbed gas has lower ionization level than the quiescent gas. They propose that the disturbed gas is outflowing as a result of interactions between the radio jets and the gas.
The velocity gradients may indicate rotation (Villar-Martín et al., 2003, 2006), gas infall (Humphrey et al., 2007b) or gas outflow Humphrey et al. (2006).
Based on a comparison with single-slab, AGN photoionization models Villar-Martín et al. (2002) found that the metallicity in this radio galaxy is close to solar. Humphrey et al. (2007a) found that on the side of the nucleus with the shortest radio lobe the ionization parameter is lower than on the other side and that the brightness of the UV and optical continuum emission and the brightness of the line emission show similar spatial asymmetries.

4.2 GENERAL RESULTS

The following images show the two dimensional spectra of TXS 0828+193. The spectra are smoothed with a gaussian function with radius of 3 pixels to better show the emission line features.

The two dimensional spectra of TXS 0828+193 are shown in Figures 4.3 and 4.4. Lyα is the brightest and most extended emission line. In the GTC spectrum (PA=$-45°$) Lyα has a total detected extent of $\sim$68 kpc (8.4″). NV has a total detected extent of $\sim$19 kpc (2.3″), CIV has a total detected extent of $\sim$43 kpc (5.3″), HeII has a total detected extent of $\sim$37 kpc (4.6″), and CIII] has a total detected extent of $\sim$31 kpc (3.8″). The detection of extended emission from metals indicates that the gas is significantly enriched in metals even far from the centre of the galaxy, consistent with previous studies of this galaxy (Villar-Martín et al., 2002).

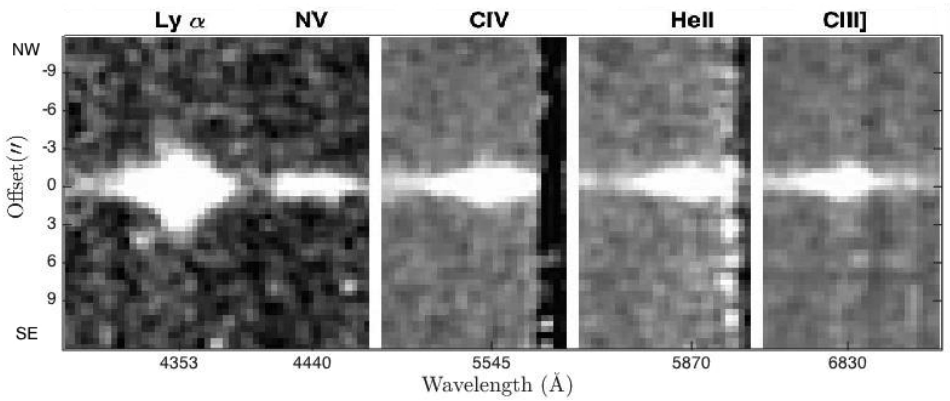

Figure 4.3: 2D spectrum of the main emission lines for TXS 0828+193, with the slit oriented perpendicularly to the radio axis. At z=2.57, 1″ corresponds to 8.144 kpc.

In the direction of the radio axis Lyα emission extends beyond the radio source ($\sim$ 130 kpc) as previously found by Villar-Martín et al. (2002). The bright continuum source at $\sim$ -4″ is an unrelated M5V star (Vernet et al., 2001).

One dimensional spectra showing different regions of TXS 0828+193 observed with the slit positioned perpendicularly to the radio axis are shown in Figure 4.5.

What seems to be an excess of emission in the blue wing of Lyα is seen in the middle and

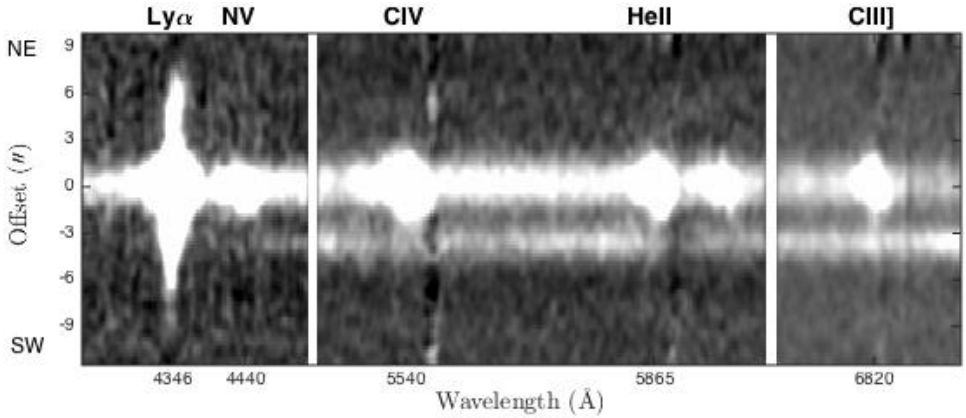

Figure 4.4: 2D spectrum of the main emission lines for TXS 0828+193, with the slit oriented in the direction of the radio axis. The zero in the spatial direction (offset) corresponds to the peak of the continuum emission.

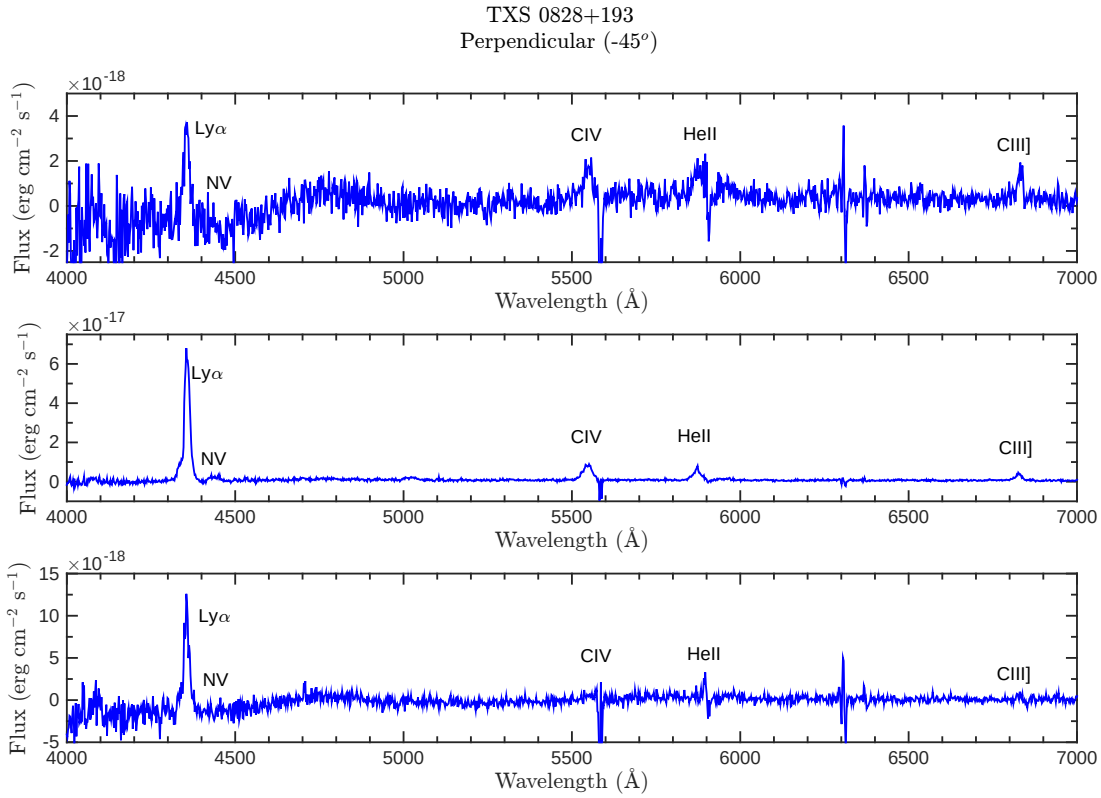

Figure 4.5: One dimensional spectra of different regions of TXS 0828+193 observed with the slit positioned perpendicularly to the radio axis. The top spectrum shows the region between -4.3″ and -1.3″, the spectrum in the middle shows the nuclear region (central 2″) and the bottom spectrum shows the region between 1.3″ and 4.6″. Lyα, NV, CIV, HeII and CIII] positions are indicated in the spectra. NV is only detected in the central region. There are some skyline residuals affecting the emission lines. CIV emission line is affected by the 5577 Å (OI) skyline, HeII is affected by a skyline at 5889 Å (Na D) and CIII] is affected by a skyline at $\sim$ 6828 Å (OH).

bottom panels of Figure 4.5.

CIV, HeII emission lines are affected by skyline residuals which may affect the kinematics

results.

4.3 EMISSION LINE FLUX MEASUREMENTS AND SPATIAL PROFILES

A comparison of the spatial profiles of the Lyα line with the spatial profile of the continuum emission is shown in Figure 4.6.

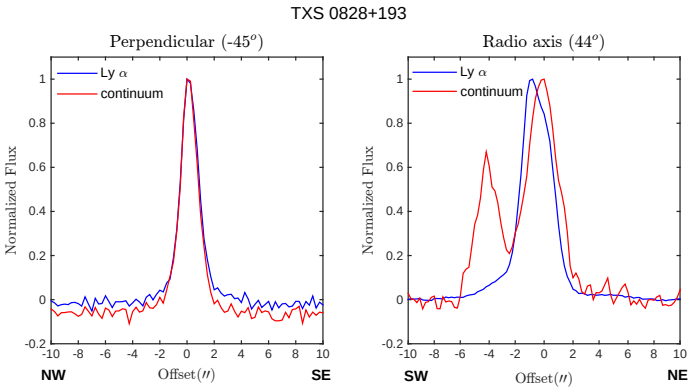

Figure 4.6: Spatial profiles of the Lyα and continuum emissions in TXS 0828+193 observed with the slit positioned perpendicularly to the radio axis (left) and along the radio axis (right).

In the direction perpendicular to the radio axis (PA=-45°) the peak of Lyα emission line and the peak of the continuum emission are coincident.
In the direction of the radio axis (PA=44°), the peak of Lyα emission line is slightly offset from the peak of the continuum emission. The second, less pronounced peak is due to a star (M5V) in our Galaxy (Vernet et al., 2001).

The spatial profiles of the emission lines are shown in Figure 4.7.

The emission in TXS 0828+193 is typical of HzRGs (e.g. McCarthy, 1993; Humphrey et al., 2008). Lyα is the brightest of the UV emission lines. The peak of the emission lines coincides with the peak of the continuum emission in most lines. The emission lines are slightly more extended in the direction of the radio axis. As already shown by Villar-Martín et al. (2002), in the observation along the radio axis Lyα extends beyond the radio structures.

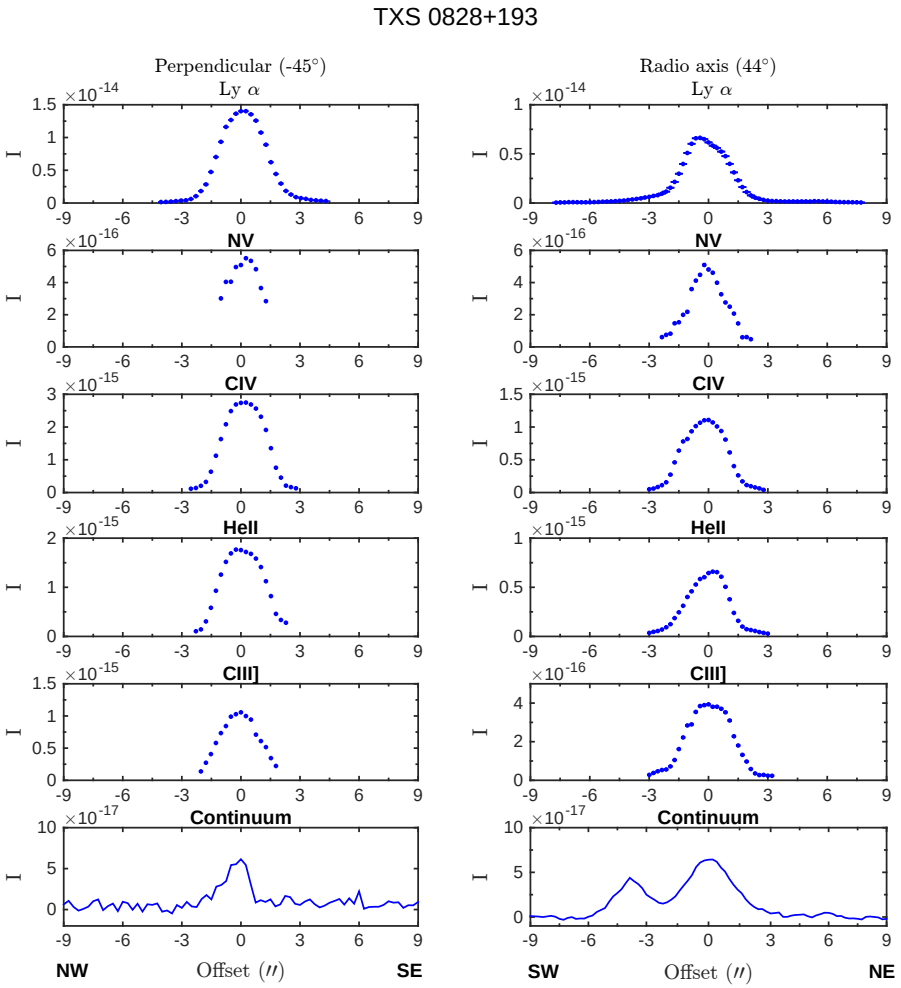

Figure 4.7: Surface brightness (I) of the different emission lines and continuum profile (bottom figures) for TXS 0828+193. The left figures are the surface brightness values observed perpendicularly to the radio axis and the right figures the flux observed along the radio axis. The surface brightness units are erg cm^{-2} s^{-1} arcsec^{-2}. Zero in the spatial direction represents the peak of the continuum emission.

4.4 LINE RATIOS AND COMPARISON WITH MODELS

Figure 4.8 shows how the different emission line ratios vary along the slit.

In the direction perpendicular to the radio axis, (Figure 4.8 left), the emission line ratios Lyα/HeII and Lyα/CIV show a peak around $\sim$ -2″. Another local maximum is seen for the same line ratios at $\sim$ 2″. This may suggest that Lyα emission is enhanced in these regions. However, it is not immediately clear whether this is due to enhanced Lyα or lower fluxes for the other lines.

In the direction of the radio axis (Figure 4.8 right) Lyα/HeII, CIII]/CIV, CIII]/HeII and maybe

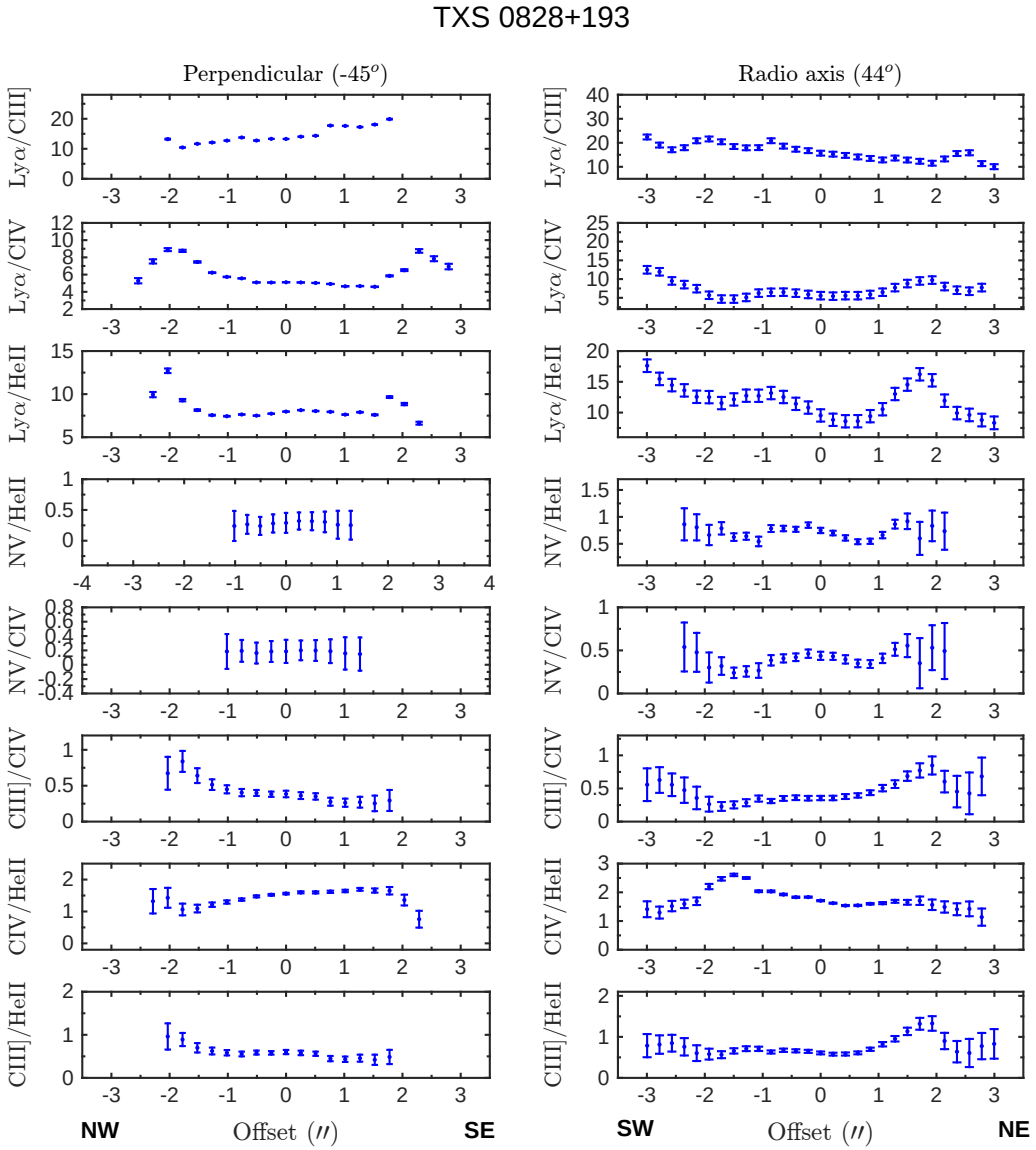

Figure 4.8: Ratios between the emission lines in TXS 0828+193 as a function of distance in the galaxy. In the left are shown the flux ratios in the direction perpendicular to the radio axis (PA=-45°) and in the right in the direction of the radio axis (PA=44°).

Lyα/CIV show a local maximum at $\sim$ 2″, but this time with only one corresponding feature at $\sim$ -2″(CIV/HeII).

A comparison is made between the results of our observations and photoionization and shock models. In order to do that several apertures were extracted along the slit. This will allow us to study the physical conditions in the different regions of the nebula.

Table 4.1 shows the different apertures and the flux ratios for the different emission lines

in the direction perpendicular to the radio axis (PA=-45°).

Pos. (1)	Lyα/HeII (2)	Lyα/CIV (3)	Lyα/CIII] (4)	CIV/HeII (5)	CIV/CIII] (6)	NV/HeII (7)	NV/CIV (8)
-4.3″ : -2.5″	2.3±0.3	3.7±0.4	-	0.6±0.4	-	-	-
-2.5″ : -1.5″	2.7±0.3	2.6±0.2	3.0±0.2	1.0±0.2	1.14±0.2	-	-
-1.5″ : 1″	7.61±0.03	4.77±0.02	14.7±0.05	1.60±0.03	3.07±0.05	0.36±0.09	0.23±0.09
1″ : 2″	-	24.6±0.3	36.7±0.3	-	1.5±0.4	-	-

Table 4.1: Emission line ratio measurements from the TXS 0828+193 spectrum, observed perpendicularly to the radio axis (PA=-45°). Columns are as follows: (1) position of the aperture along the slit in arcseconds; (2) the Lyα/HeII ratio; (3) the Lyα/CIV ratio; (4) the Lyα/CIII] ratio; (5) the CIV/HeII ratio; (6) the CIV/CIII] ratio; (7) the NV/HeII ratio; (9) the NV/CIV ratio.

Pos. (1)	Lyα/HeII (2)	Lyα/CIV (3)	Lyα/CIII] (4)	CIV/HeII (5)	CIV/CIII] (6)	NV/HeII (7)	NV /CIV (8)
-3.6″ : -1.3″	19.39±0.08	8.94±0.04	16.33±0.06	2.2±0.1	1.83±0.07	0.6±0.2	0.3±0.2
-1.3″ : 0.9″	10.85±0.01	5.90±0.01	19.91±0.02	1.84±0.01	3.37±0.02	0.56±0.04	0.30±0.04
0.9″ : 2.8″	8.3±0.03	5.22±0.02	20.92±0.06	1.60±0.04	4.01±0.06	0.3±0.2	0.3±0.2
2.8″ : 3.6″	6.5±0.2	5.0±0.2	-	1.3±0.2	-	-	-

Table 4.2: Emission line ratio measurements from the TXS 0828+193 spectrum, observed along the radio axis (PA=44°). Columns are as in table 4.1.

In table 4.2 it can be seen that in the outer regions of the nebula Lyα emission is very bright in comparison to HeII, CIV and CIII]. The ratio CIII]/CIV suggest that the state of ionization of the gas is not constant but varies across the nebula. The ratio CIV/HeII suggests an increase in the ionization state of the gas, from NE ($\sim$ 3.6″) to SW ($\sim$ -3.6″). This result is in agreement with results from Humphrey et al. (2007a). NE corresponds to the position of the shorter radio lobe.

To help distinguish between ionization mechanisms in the gas line-ratio diagrams were used. The models are the same as used for TXS 0211-122.

In Figure 4.9 diagrams showing photoionization and shock models for the slit perpendicular to the radio axis are shown.

It is seen in Figure 4.9 that a MAPPINGS 1e photoionization model with 3 times solar metallicity is able to reproduce the ratios for the region -2.5″ to -1.5″ in some diagrams. However the ratios are also reproduced by shock and shock plus precursor models. The emission line ratios obtained for the centre of the galaxy, which correspond to the region between -1.5″ and 1″ are reproduced by a photoionization grid with Z=3Z$_\odot$ or Z=Z$_\odot$ or by the shock plus precursor model. This suggests that in the centre of the galaxy there is high

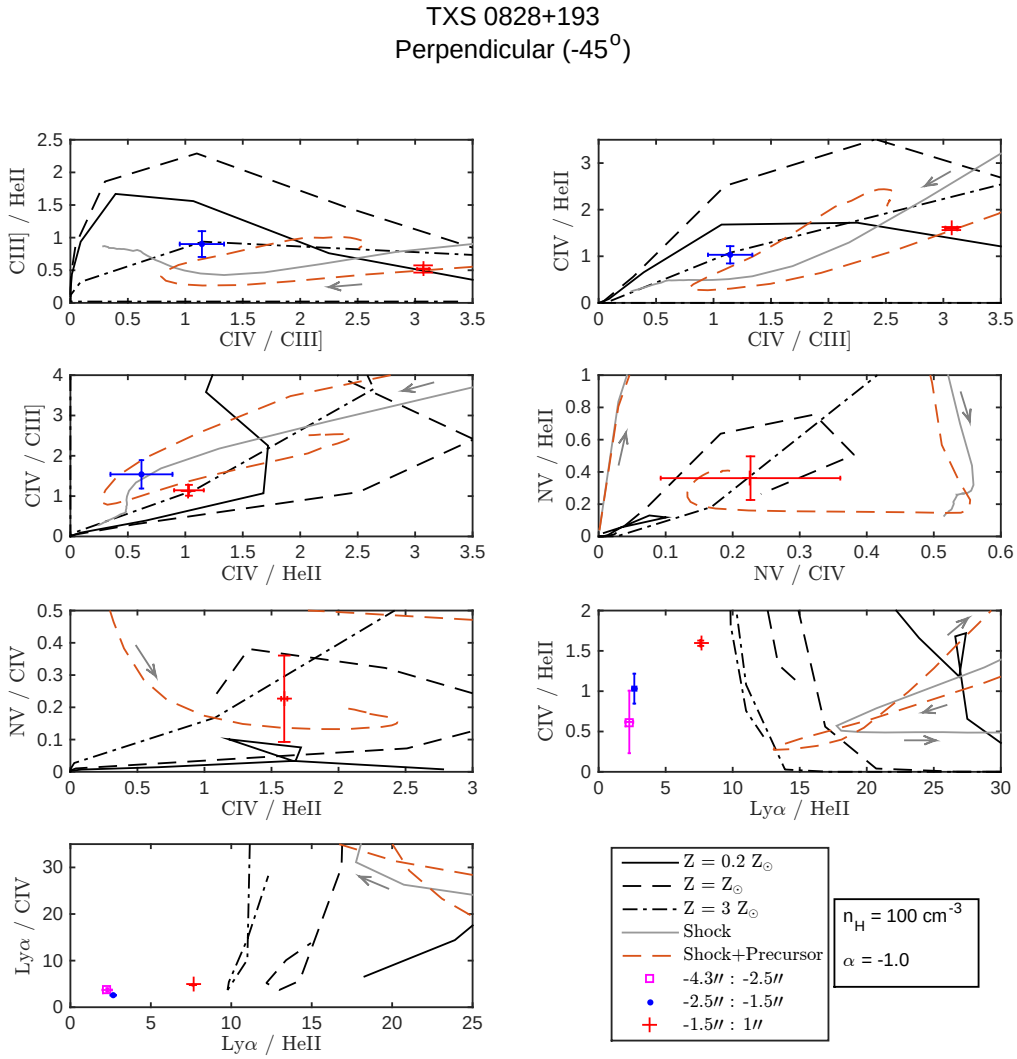

Figure 4.9: Flux ratios of TXS 0828+193 observed with the slit in the position perpendicular to the radio axis plotted on diagnostic diagrams involving CIV, HeII and CIII]. Shock models by Allen et al. (2008) and MAPPINGS photoionization models are shown. Grey solid lines denote the predictions of pure shock models, and orange-dotted lines denote the prediction of shock plus precursor models. The parameters are the same for all figures. The arrows indicate the direction of increasing velocity.

metallicity and/or that jet-gas interactions are heating the gas.

Due to the low Lyα/HeII ratio we observe the models are not able to reproduce our results. This ratio is low because HeII is strong, which can also be seen in the ratio CIV/HeII that is always lower than 1.75, the typical value for CIV/HeII in HzRGs (Humphrey et al., 2008). The detection of strong HeII emission strongly disfavours photoionization by young stars and resonant scattering as powering mechanisms.

In Figure 4.10 diagrams showing photoionization and shock models for the slit along the radio axis are shown.

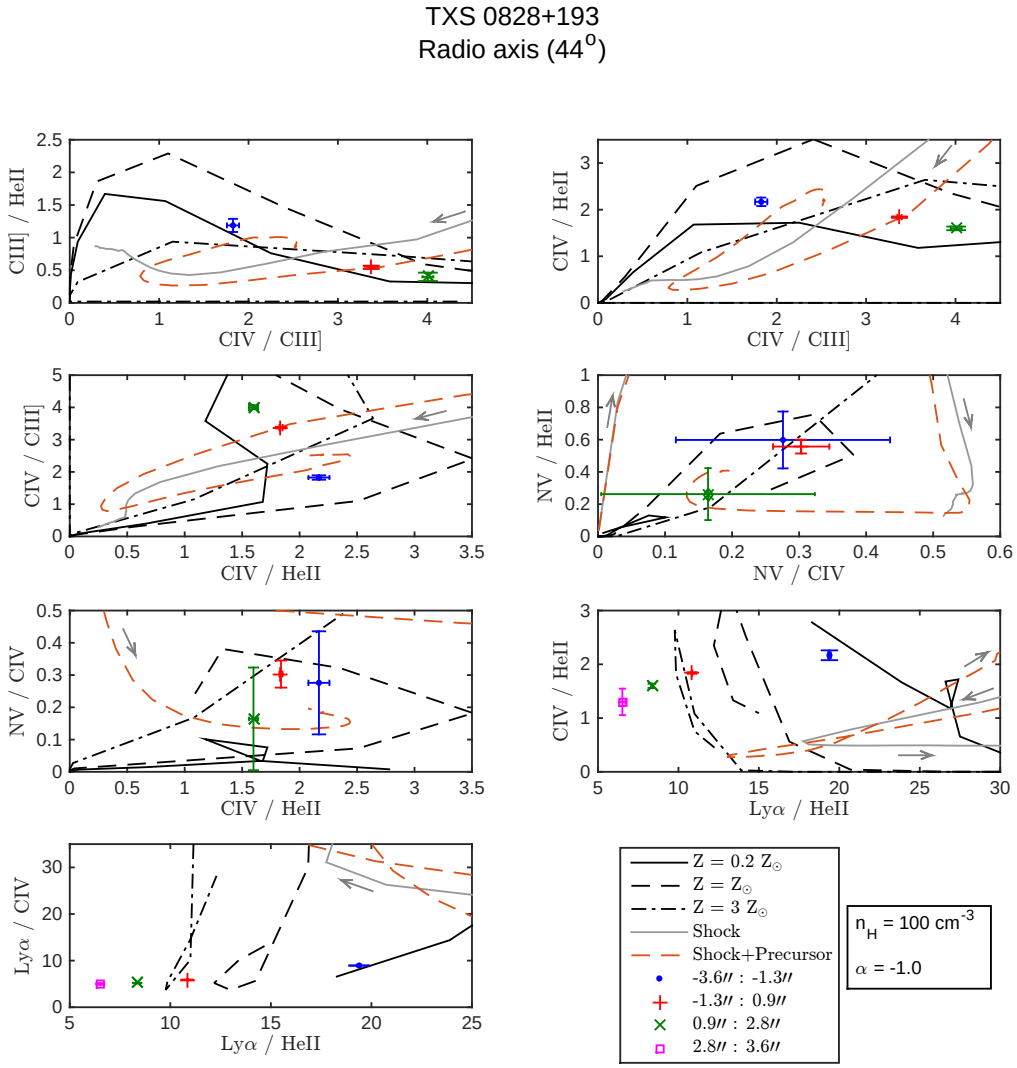

Figure 4.10: Flux ratios observed with the slit along the radio axis plotted on diagnostic diagrams involving CIV, HeII and CIII]. MAPPINGS photoionization models are shown. Shock models by Allen et al. (2008) are also shown. Grey solid lines denote the predictions of pure shock models, and orange-dotted lines denote the prediction of shock plus precursor models. The parameters are the same for all figures. The arrows indicate the direction of increasing velocity.

The diagram of NV/HeII versus NV/CIV suggests that the gas metallicity is high. Photoionization models with metallicities between $Z_\odot$ and $3Z_\odot$ give the best representation of the results. The diagram NV/HeII versus NV/CIV shows that photoionization with $3Z_\odot$ and a sequence in ionization parameter is able to reproduce our results in the apertures -3.6″ to -1.3″, -1.3″ to 0.9″, and 0.9″ to 2.8″.

In the direction of the radio axis (PA=44°) shocks may make some contribution to the heating of the gas, however, as Villar-Martín et al. (2002) have already shown, the detection

of emission lines beyond the radio structure is evidence that photoionization by the AGN is the main ionization mechanism in this direction.

The conclusions from the comparison between observed line ratios and models should be considered indicative. Models with a higher range of model parameter space are needed to determine more accurate gas chemical abundances.

4.5 KINEMATICS

The velocity curves of Lyα, CIV and HeII are shown in Figure 4.11.

Perpendicularly to the radio axis HeII is only detected in the inner regions of the nebula and its velocity is near systemic (within the error bars). In the same region CIV also presents near systemic velocities. In the outer regions, the CIV velocity profile closely resembles the velocity profile of Lyα.
In the centre of the galaxy Lyα emission is being redshifted ($v_{Ly\alpha} \sim 350$ km s^{-1}). The modulus of the maximum difference in radial velocity of HeII is Δv(HeII) $\sim$ 160 km s^{-1}, for CIV the maximum difference in radial velocity Δv(CIV) $\sim$ 180 km s^{-1}.

There is a velocity shift ($\sim$ 350 km s^{-1} for PA=-45°, and $\sim$ 220 km s^{-1} for PA=44°) between Lyα and HeII. There are at least two possible reasons for this. First, Lyα and HeII may originate in gas from different locations, and thus different kinematic properties, in the overall nebulosity. Secondly, a large fraction of HzRG show the presence of HI absorption of Lyα emission (van Ojik et al., 1997) resulting in a redshift of the peak of the Lyα emission (when observed at low resolution). Therefore HI absorption systems may play a role in producing the observed velocity shifts (Röttgering et al., 1995).
Velocity shifts between emission lines have been reported by numerous studies of powerful radio galaxies (McCarthy et al., 1990; Tadhunter, 1991). In some cases the authors have proposed that the shifts could be related to the AGN (Tadhunter, 1991), or to inflow or outflow on the near side of the galaxy, with obscuration of the emission from the other side (Eales et al., 1993).

In the direction perpendicular to the radio axis (PA=-45°) Lyα emission (Figure 4.11) from the central regions show an approximately constant redshifted velocity relatively to HeII. In this direction there are some changes in the velocity pattern at $\sim$ -2″ and $\sim$ 2″. Signs of a difference in the velocity curve close to these regions are also seen in CIV.

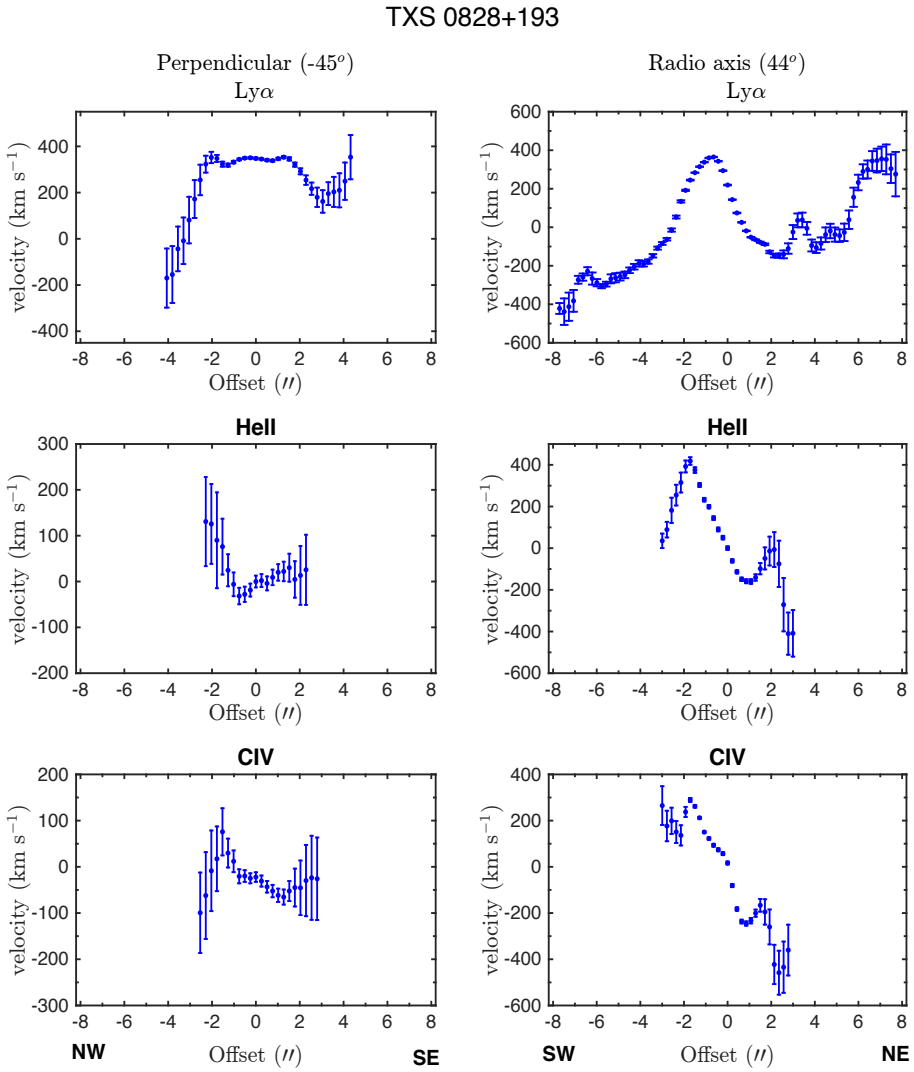

Figure 4.11: Lyα (top), HeII (middle) and CIV (bottom) velocity profiles for TXS 0828+193. The left figures represent the variation in the direction perpendicular to the radio axis, while the right plots represent the variation along the radio axis.

In the direction of the radio axis (PA=44°) the Lyα emission is being blueshifted in some regions and redshifted in other regions (Figure 4.11 top right). HeII and CIV show similar velocity curves. At ∼ -2″ and ∼ 2″ CIV and HeII show local maxima in their velocity curves.

Figure 4.12 shows the FWHMs of the line emission as a function of distance from the nucleus.

In the direction perpendicular to the radio axis (PA=-45°) the emission lines show large FWHMs (> 1000 km s^{-1}). CIV is broad in the central regions but becomes narrower at ∼ -2″ and ∼ 2″.

In the direction of the radio axis (PA=44°) the FWHM(Lyα) shows lower FWHMs on the side

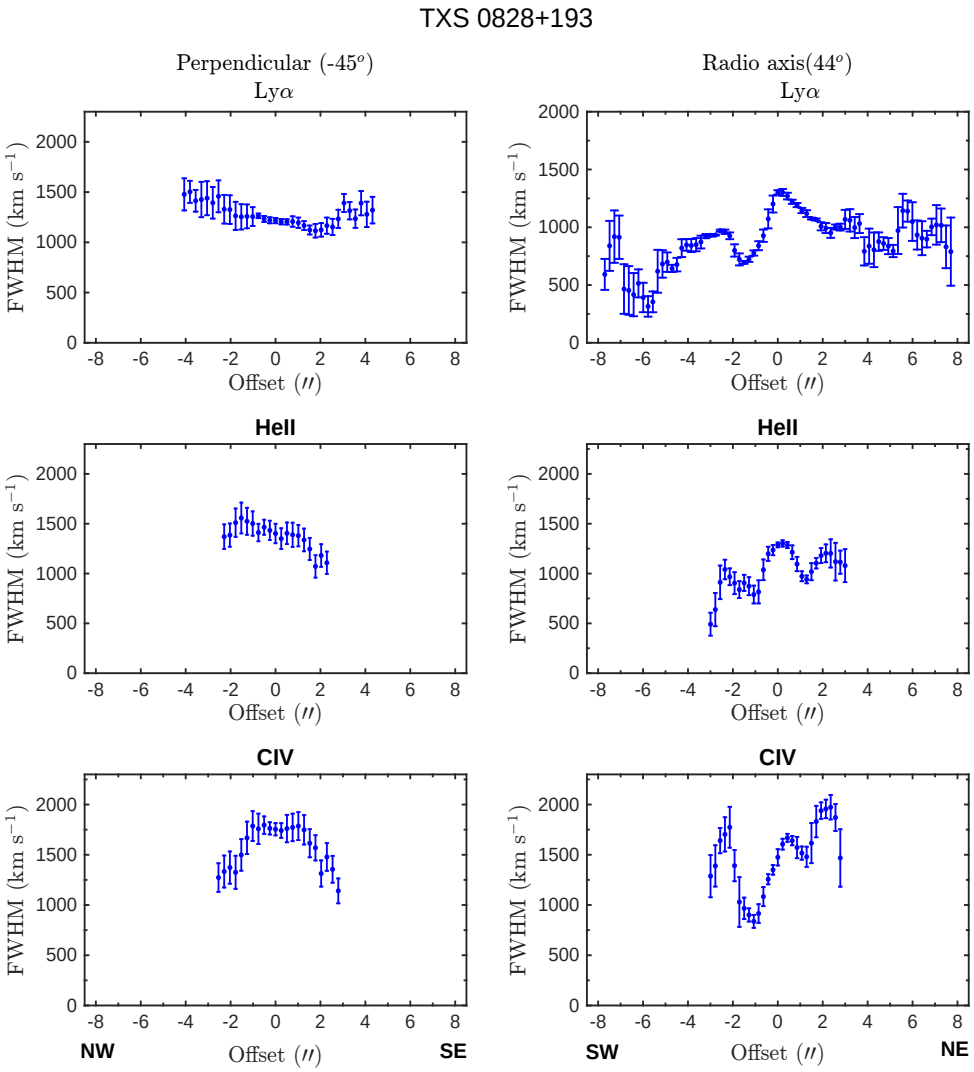

Figure 4.12: FWHM for TXS 0828+193 observed in the direction perpendicular to the radio axis (left) and in the direction of the radio axis (right).

of the southwestern lobe suggesting that that region has quiescent kinematics.

High velocity dispersions have previously been attributed to interactions between the radio source and the emission line gas (McCarthy et al., 1990; Chambers et al., 1990). They may also have a gravitational origin if gas in falling from large radii (Fall and Rees, 1985). Gas falling in from large radii can have FWHM of more than 1000 km s^{-1} and velocities of $\sim$ 500 km s^{-1} (Heckman et al., 1991).

It is difficult to discriminate between different kinematic scenarios. Rotation, infall and outflows can produce similar velocity patterns (McCarthy, 1993). However, Humphrey et al. (2006) found outflowing gas resulting from jet-gas interactions in this galaxy, and the kinematics of the gas in the direction perpendicular to the radio axis (PA=-45°) may also be due

to interactions between the jets and the gas. The following section discusses a scenario that possibly explains the observations.

Outflows

Gas outflows in HzRGs have been attributed to starbursts (Nesvadba et al., 2007), AGN winds (Nesvadba et al., 2008) and to the interaction between the jets and the gas (Villar-Martín et al., 2003; Humphrey et al., 2006). However, due to several evidences for jet-gas interactions in this galaxy (Villar-Martín et al., 2002; Humphrey et al., 2006; Nesvadba et al., 2008) it is assumed that the outflows are due to this type of interaction.

One of the evidences for jet-gas interactions is that in the direction of the radio axis (PA=44°) many of the UV lines show a perturbed, blueshifted component coincident with the extent of the radio emission. Another evidence is that the region with the lowest ionization state is to the side of the shortest radio lobe (Humphrey et al., 2007a).

The large FWHM seen in the direction perpendicular to the radio axis is evidence that the disturbed emission line kinematics are not confined to the radio axis. Relatively broad lines in Lyα are detected out to a radial distance of $\sim$ 35 kpc from the nucleus. In the slit perpendicular to the radio axis (PA=-45°) the line ratios involving Lyα/CIV and Lyα/HeII show local peaks at approximately $\pm 2''$. High FWHM are seen for Lyα, CIV and HeII along the slit. A change in the velocity curve of Lyα is seen at approximately $\pm 2''$.
In the direction of the radio axis (PA=44°) line ratios involving Lyα/HeII, Lyα/CIII], CIII]/HeII, CIII]/HeII and maybe Lyα/CIV show local peaks at $\sim 2''$. The velocity curves of HeII and CIV show a change in the velocity at approximately $\pm 2''$, and CIV becomes narrower at radii beyond 2 from the centre.
Summing up, there seems to be an enhancement in the emission of several lines and a change in the velocity pattern at $\pm 2''$ from the nucleus, suggesting the presence of a circumnuclear mechanism operating at r $\sim 2''$ that is disturbing the gas and altering its excitation properties.
In order to try to explain the observations a simple scenario was developed. The scenario consists of an expanding bubble of gas with a radius of $\sim 2''$ (see Fig. 4.13). The expanding bubble may have perturbed the gas inside the $2''$ radius ($\sim$ 16 kpc) and the gas is more quiescent outside resulting in the difference of FWHM(CIV) observed in the perpendicular slit.

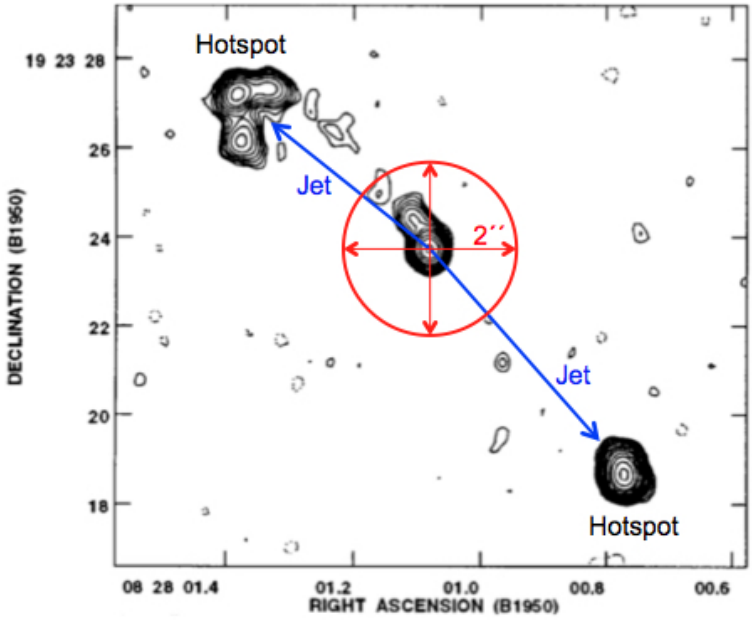

Figure 4.13: Expanding bubble scheme overplotted in the image of the full field of TXS 0828+193 taken from Carilli et al. (1997).

To see if the bubble and the hotspots could have been triggered by the same mechanism the age of each source was calculated. In order to do that a few assumptions had to be made. Knowing that the average speed of hotspot advance is $\sim$ 0.01 - 0.4c (e.g. Carilli et al., 1991; Liu et al., 1992; Best et al., 1995; Arshakian and Longair, 2000) it was assumed that the hotspots had velocities of 0.01c. The distance from the AGN to the hotspots is $\sim$ 50 kpc (approximately half the size of the radio source).
Typical velocity values of starburst driven galactic superwinds are several hundred km s^{-1} (Bland and Tully, 1988; Heckman, 2003) therefore for the bubble an expansion velocity of 1000 km s^{-1} was adopted. The radius of the bubble is $\sim$ 16 kpc ($\sim 2''$).
Assuming the aforementioned values it was found that the age of the bubble and the age of the hotspots are approximately the same, $\sim 2 \times 10^7$ years. This means that they could have been triggered by the same mechanism (AGN), or the could have been triggered by different mechanisms that started at the same time. For example, if a merger occurred in the past, the gas could have been used to fuel the AGN which could trigger both the jet (and, consequently the hotspots), and the bubble of gas. Instead of being driven by the AGN the expanding bubble of gas could be due to winds and supernovae starbursts (e.g. Heckman et al., 1990) close to the nucleus of the galaxy.

It is important to stress that the scenario developed above is based on a number of assumptions, and is not necessarily the only way to explain the observations.

Chapter 5

Conclusions

The study of active galaxies at high redshift is crucial to fully understand the formation and evolution of galaxies. In particular, HzRGs are useful probes of the formation and evolution of massive galaxies, and give the opportunity to study galaxies during a phase of intense AGN activity.

This thesis has presented new spectroscopic observations of two HzRGs, TXS 0211-122 and TXS 0828+193, observed with long-slits positioned perpendicularly to the radio axis. This is the first time that the two galaxies have been observed with a long-slit positioned in the direction perpendicular to the radio axis. This technique represents an observationally inexpensive alternative to IFU spectroscopy, and can be particularly useful for HzRGs whose redshift would place Lyα blueward of the wavelength range of MUSE. These observations allow us to compare the properties of the gas in different regions of the galaxy.

In both galaxies Lyα halos are detected in the direction perpendicular to the radio axis. In this direction it is highly unlikely that the emission lines are being illuminated by the central AGN raising the possibility that mechanisms other than AGN photoionization may be responsible for exciting the gas.

TXS 0211-122

- TXS 0211-122 shows an extended Lyα emission halo in the direction perpendicular to the radio axis ($\sim$61 kpc).

- The presence of NV, CIV, HeII and CIII] in the extended regions in the perpendicular slit indicates that the gas is ionized and enriched with heavy elements.
- A continuum source, from which no emission lines are detected, is detected northward of the centre of the galaxy, close to the edge Lyα halo. Using Keck II observations Humphrey et al. (2013) detected a pair of diametrically opposed continuum sources with similar properties. The distances between the continuum sources and the centre of the radio galaxy are approximately the same in their work and in this one, approximately 7″ ($\sim$ 58 kpc). This result suggest that the sources are manifestations of an arc-like feature, surrounding the Lyα halo. The fact that these sources are detected close to the edge of the Lyα nebula suggests a physical connection with the Lyα halo. At this point the cause of the connection (if there is one) is not clear.
- The line ratios in the direction perpendicular to the radio axis suggest high levels of chemical enrichment of the gas, with a metallicity of $3Z_{\odot}$. The observations in both PAs suggest that the gas metallicity is high and that Lyα is being strongly absorbed.
- HI absorption and/or scattering is strongly affecting the velocity curve of Lyα in the perpendicular slit. HeII shows quiescent kinematics along this PA.
- We find evidence for outflowing gas in the direction of the radio axis. In the perpendicular slit we did not find any evidence of the existence of outflowing gas. This suggests that the outflowing gas is preferentially situated along the radio axis and may be due to jet-gas interactions.

TXS 0828+193

- A Lyα halo, with total extent of $\sim$ 68 kpc is detected in the direction perpendicular to the radio axis. Besides Lyα, the emission lines NV, CIV, HeII and CIII] are along this position angle.
- The detection of strong HeII emission in the slit perpendicular to the radio axis indicates that neither resonant scattering nor photoionization by young stars are responsible for powering the extended line emission. In this direction the gas is probably not photoionized by the AGN therefore the ionization mechanism is most likely shocks. In the direction of the radio axis shocks may also play a role in heating the gas but the main ionization mechanism is photoionization by the AGN.
- The presence of an excess of emission in the blue wing of Lyα is indicative of outflows. The high FWHM of Lyα, CIV and HeII observed in both PAs suggest that the gas is

being perturbed, in agreement with previous studies (e.g. Villar-Martín et al., 2002). In the perpendicular slit, diametrically opposed maxima in Lyα/CIV and Lyα/HeII are detected at a radii of $\sim 2''$ ($\sim$ 16 kpc), with a corresponding maxima also seen in the slit positioned along the radio axis. In addition, the kinematic properties of several lines appear correlated with these maxima, with CIV evolving from perturbed at r < $2''$ to quiescent at r > $2''$ and several lines showing sharp velocity shifts there. This may be the result of a spherical shell or bubble of gas. The detection of kinematic changes and peaks in several emission line ratios at $\pm 2''$ suggest that the outflowing gas has approximately spherical distribution, with perturbed gas inside and more relaxed gas outside. Since there are several evidences for jet-gas interactions in this galaxy the gas may be perturbed by this mechanism. We found evidence for outflowing gas with an approximately spherical distribution that may be due to presence of an expanding bubble of gas.

Chapter 6

Future Work

Further spectroscopic observations of HzRGs are needed to determine the properties of the gas in HzRGs. Until now, much has been learnt about HzRGs and their gaseous components but much more remains to be understood.
3D studies of AGN and their environments are essential to study feedback processes. Integral field spectroscopy would be useful to map the morphology and physical conditions across the entire Lyα halo.

Deep imaging of TXS 0211-122 would be very useful to determine the morphology, and thus origin, of the offset continuum sources. Combination of ALMA and VLT observations could be useful to obtain a complete view of the AGN and its environment in order to detect closer companions and merger events and assess the molecular gas content of the host galaxies.

HST or adaptive optics imaging would be useful to study the nature of the apparently spherical structure detected at r $\sim 2''$ in TXS 0828+193.

At higher redshift, deep spectroscopic observations with the MUSE integral-field unit that map the two-dimensional kinematics of Lyα nebulae will be very useful to differentiate between different origins of the kinematics in the Lyα halo.

Future observations of HzRGs embedded in Lyα nebulae may finally give us the answer to the nature of the Lyα halos and their connection with the formation and evolution of massive galaxies.

Bibliography

Allen, M. G., Groves, B. A., Dopita, M. A., Sutherland, R. S., and Kewley, L. J. The MAPPINGS III Library of Fast Radiative Shock Models. *ApJS*, 178:20–55, Sept. 2008. doi: 10.1086/589652.

Arshakian, T. G. and Longair, M. S. An asymmetric relativistic model for classical double radio sources. *MNRAS*, 311:846–860, Feb. 2000. doi: 10.1046/j.1365-8711.2000.03098.x.

Asplund, M., Grevesse, N., and Jacques Sauval, A. The solar chemical composition. *Nuclear Physics A*, 777:1–4, Oct. 2006. doi: 10.1016/j.nuclphysa.2005.06.010.

Athreya, R. M., Kapahi, V. K., McCarthy, P. J., and van Breugel, W. Large rotation measures in radio galaxies at Z > 2. *A&A*, 329:809–820, Jan. 1998.

Baldwin, J. A., Phillips, M. M., and Terlevich, R. Classification parameters for the emission-line spectra of extragalactic objects. *PASP*, 93:5–19, Feb. 1981. doi: 10.1086/130766.

Begelman, M. and Rees, M. *Gravity's fatal attraction. Black holes in the universe*. 1996.

Best, P. N., Bailer, D. M., Longair, M. S., and Riley, J. M. Radio source asymmetries and unified schemes. *MNRAS*, 275:1171–1184, Aug. 1995. doi: 10.1093/mnras/275.4.1171.

Bicknell, G. V., Sutherland, R. S., van Breugel, W. J. M., et al. Jet-induced Emission-Line Nebulosity and Star Formation in the High-Redshift Radio Galaxy 4C 41.17. *ApJ*, 540: 678–686, Sept. 2000. doi: 10.1086/309343.

Binette, L., Dopita, M. A., and Tuohy, I. R. Radiative shock-wave theory. II - High-velocity shocks and thermal instabilities. *ApJ*, 297:476–491, Oct. 1985. doi: 10.1086/163544.

Bland, J. and Tully, B. Large-scale bipolar wind in M82. *Nature*, 334:43–45, July 1988. doi: 10.1038/334043a0.

Blandford, R. D. and Rees, M. J. A 'twin-exhaust' model for double radio sources. *MNRAS*, 169:395–415, Dec. 1974.

Blumenthal, G. and Miley, G. Spectral index dependent properties of steep spectrum radio sources. *A&A*, 80:13–21, Nov. 1979.

Blundell, K. M., Rawlings, S., and Willott, C. J. The Nature and Evolution of Classical Double Radio Sources from Complete Samples. *AJ*, 117:677–706, Feb. 1999. doi: 10.1086/300721.

Bower, R. G., Benson, A. J., Malbon, R., et al. Breaking the hierarchy of galaxy formation. *MNRAS*, 370:645–655, Aug. 2006. doi: 10.1111/j.1365-2966.2006.10519.x.

Cano-Díaz, M., Maiolino, R., Marconi, A., et al. Observational evidence of quasar feedback quenching star formation at high redshift. *A&A*, 537:L8, Jan. 2012. doi: 10.1051/0004-6361/201118358.

Carilli, C. L., Perley, R. A., Dreher, J. W., and Leahy, J. P. Multifrequency radio observations of Cygnus A - Spectral aging in powerful radio galaxies. *ApJ*, 383:554–573, Dec. 1991. doi: 10.1086/170813.

Carilli, C. L., Röttgering, H. J. A., van Ojik, R., et al. Radio Continuum Imaging of High-Redshift Radio Galaxies. *ApJS*, 109:1–44, 1997. doi: 10.1086/312973.

Cattaneo, A., Faber, S. M., Binney, J., et al. The role of black holes in galaxy formation and evolution. *Nature*, 460:213–219, July 2009. doi: 10.1038/nature08135.

Chambers, K. C., Miley, G. K., and van Breugel, W. Alignment of radio and optical orientations in high-redshift radio galaxies. *Nature*, 329:604–606, Oct. 1987. doi: 10.1038/329604a0.

Chambers, K. C., Miley, G. K., and van Breugel, W. J. M. 4C 41.17 - A radio galaxy at a redshift of 3.8. *ApJ*, 363:21–39, Nov. 1990. doi: 10.1086/169316.

Charlot, S. and Fall, S. M. Attenuation of Lyman-alpha emission by dust in damped Lyman-alpha systems. *ApJ*, 378:471–475, Sept. 1991. doi: 10.1086/170448.

De Breuck, C., Röttgering, H., Miley, G., van Breugel, W., and Best, P. A statistical study of emission lines from high redshift radio galaxies. *A&A*, 362:519–543, Oct. 2000.

De Breuck, C., van Breugel, W., Röttgering, H., and Carilli, C. Radio AGN Surveys. In Green, R. F., Khachikian, E. Y., and Sanders, D. B., editors, *IAU Colloq. 184: AGN Surveys*, volume 284 of *Astronomical Society of the Pacific Conference Series*, page 275, 2002.

De Breuck, C., Seymour, N., Stern, D., et al. The Spitzer High-redshift Radio Galaxy Survey. *ApJ*, 725:36–62, Dec. 2010. doi: 10.1088/0004-637X/725/1/36.

Douglas, J. N., Bash, F. N., Torrence, G. W., and Wolfe, C. The Texas Survey - Preliminary + 18DEG Strip. *University of Texas Publications in Astronomy*, 17:1, 1980.

Dubinski, J. The Origin of the Brightest Cluster Galaxies. *ApJ*, 502:141–149, July 1998. doi: 10.1086/305901.

Duval, F., Schaerer, D., Östlin, G., and Laursen, P. Lyman α line and continuum radiative transfer in a clumpy interstellar medium. *A&A*, 562:A52, Feb. 2014. doi: 10.1051/0004-6361/201220455.

Eales, S., Rawlings, S., Puxley, P., Rocca-Volmerange, B., and Kuntz, K. Evidence that the Z = 3.4 radio galaxy B2 0902+34 may be a protogalaxy. *Nature*, 1993.

Fall, S. M. and Rees, M. J. A theory for the origin of globular clusters. *ApJ*, 298:18–26, Nov. 1985. doi: 10.1086/163585.

Ferrarese, L. and Merritt, D. A Fundamental Relation between Supermassive Black Holes and Their Host Galaxies. *ApJ*, 539:L9–L12, Aug. 2000. doi: 10.1086/312838.

Ferruit, P., Binette, L., Sutherland, R. S., and Pecontal, E. Modeling extragalactic bow-shocks. I. The model. *A&A*, 322:73–85, June 1997.

Fosbury, R. A. E., Boksenberg, A., Snijders, M. A. J., et al. Very extended ionized gas in radio galaxies. I - A radio, optical and ultraviolet study of PKS 2158-380. *MNRAS*, 201: 991–1008, Dec. 1982.

Fosbury, R. A. E., Vernet, J., Villar-Martín, M., et al. The N V/C IV Ratio in High Redshift Radio Galaxies. In Walsh, J. R. and Rosa, M. R., editors, *Chemical Evolution from Zero to High Redshift*, page 227, 1999.

Gebhardt, K., Bender, R., Bower, G., et al. A Relationship between Nuclear Black Hole Mass and Galaxy Velocity Dispersion. *ApJ*, 539:L13–L16, Aug. 2000. doi: 10.1086/312840.

Groves, B. A., Dopita, M. A., and Sutherland, R. S. Dusty, Radiation Pressure-Dominated Photoionization. I. Model Description, Structure, and Grids. *ApJS*, 153:9–73, July 2004. doi: 10.1086/421113.

Hamann, F. and Ferland, G. The Chemical Evolution of QSOs and the Implications for Cosmology and Galaxy Formation. *ApJ*, 418:11, Nov. 1993. doi: 10.1086/173366.

Hartmann, L. W., Huchra, J. P., Geller, M. J., O'Brien, P., and Wilson, R. Lyman-alpha emission in star-forming galaxies. *ApJ*, 326:101–109, Mar. 1988. doi: 10.1086/166072.

Heckman, T. M. Starburst-Driven Galactic Winds. In Avila-Reese, V., Firmani, C., Frenk, C. S., and Allen, C., editors, *Revista Mexicana de Astronomia y Astrofisica Conference Series*, volume 17 of *Revista Mexicana de Astronomia y Astrofisica Conference Series*, pages 47–55, June 2003.

Heckman, T. M., Armus, L., and Miley, G. K. On the nature and implications of starburst-driven galactic superwinds. *ApJS*, 74:833–868, Dec. 1990. doi: 10.1086/191522.

Heckman, T. M., Lehnert, M. D., Miley, G. K., and van Breugel, W. Spectroscopy of spatially extended material around high-redshift radio-loud quasars. *ApJ*, 381:373–385, Nov. 1991. doi: 10.1086/170660.

Henry, R. B. C., Edmunds, M. G., and Köppen, J. On the Cosmic Origins of Carbon and Nitrogen. *ApJ*, 541:660–674, Oct. 2000. doi: 10.1086/309471.

Hopkins, P. F., Hernquist, L., Cox, T. J., et al. A Unified, Merger-driven Model of the Origin of Starbursts, Quasars, the Cosmic X-Ray Background, Supermassive Black Holes, and Galaxy Spheroids. *ApJS*, 163:1–49, Mar. 2006. doi: 10.1086/499298.

Humphrey, A., Villar-Martín, M., Fosbury, R., Vernet, J., and di Serego Alighieri, S. Jet-gas interactions in z $\sim$ 2.5 radio galaxies: evolution of the ultraviolet line and continuum emission with radio morphology. *MNRAS*, 369:1103–1114, July 2006. doi: 10.1111/j.1365-2966.2006.10224.x.

Humphrey, A., Iwamuro, F., Villar-Martín, M., et al. UV and optical emission lines from the z $\sim$ 2.6 radio galaxy 0828+193: spatially resolved measurements. *MNRAS*, 2007a.

Humphrey, A., Villar-Martín, M., Fosbury, R., et al. Giant Lyα nebulae around z > 2 radio galaxies: evidence for infall. *MNRAS*, 2007b.

Humphrey, A., Villar-Martín, M., Vernet, J., et al. Deep spectroscopy of the FUV-optical emission lines from a sample of radio galaxies at z $\sim$ 2.5: metallicity and ionization. *MNRAS*, 383:11–40, Jan. 2008. doi: 10.1111/j.1365-2966.2007.12506.x.

Humphrey, A., Vernet, J., Villar-Martín, M., et al. Polarized Extended Lyα Emission from a z = 2.3 Radio Galaxy. *ApJ*, 768:L3, May 2013. doi: 10.1088/2041-8205/768/1/L3.

Inskip, K. J., Best, P. N., Rawlings, S., et al. Deep spectroscopy of z $\sim$ 1 6C radio galaxies - I. The effects of radio power and size on the properties of the emission-line gas. *MNRAS*, 337:1381–1406, Dec. 2002. doi: 10.1046/j.1365-8711.2002.06012.x.

Ivison, R. J., Morrison, G. E., Biggs, A. D., et al. Interferometric imaging of the high-redshift radio galaxy, 4C60.07: an SMA, Spitzer and VLA study reveals a binary AGN/starburst. *MNRAS*, 390:1117–1126, Nov. 2008. doi: 10.1111/j.1365-2966.2008.13811.x.

Kauffmann, G. and Charlot, S. The K-band luminosity function at z=1: a powerful constraint on galaxy formation theory. *MNRAS*, 297:L23, June 1998. doi: 10.1046/j.1365-8711.1998.01708.x.

Kauffmann, G. and Haehnelt, M. A unified model for the evolution of galaxies and quasars. *MNRAS*, 311:576–588, Jan. 2000. doi: 10.1046/j.1365-8711.2000.03077.x.

Klamer, I. J., Ekers, R. D., Bryant, J. J., et al. A search for distant radio galaxies from SUMSS and NVSS - III. Radio spectral energy distributions and the z-α correlation. *MNRAS*, 371: 852–866, Sept. 2006. doi: 10.1111/j.1365-2966.2006.10714.x.

Kormendy, J. and Richstone, D. Inward Bound—The Search For Supermassive Black Holes In Galactic Nuclei. *ARA&A.*, 33:581, 1995. doi: 10.1146/annurev.aa.33.090195.003053.

Krolik, J. H. and Chen, W. Steep radio spectra in high-redshift radio galaxies. *AJ*, 102: 1659–1662, Nov. 1991. doi: 10.1086/115985.

Kunth, D., Lequeux, J., Sargent, W. L. W., and Viallefond, F. Is there primordial gas in IZw 18? *A&A*, 282:709–716, Feb. 1994.

Legrand, F., Kunth, D., Mas-Hesse, J. M., and Lequeux, J. Evidences for an expanding shell in the blue compact dwarf galaxy Haro 2. *A&A*, 326:929–935, Oct. 1997.

Liu, R., Pooley, G., and Riley, J. M. Spectral ageing in a sample of 14 high-luminosity double radio sources. *MNRAS*, 257:545–571, Aug. 1992. doi: 10.1093/mnras/257.4.545.

Magorrian, J., Tremaine, S., Richstone, D., et al. The Demography of Massive Dark Objects in Galaxy Centers. *AJ*, 115:2285–2305, June 1998. doi: 10.1086/300353.

McCarthy, P. J. High redshift radio galaxies. *ARA&A.*, 31:639–688, 1993. doi: 10.1146/annurev.aa.31.090193.003231.

McCarthy, P. J., van Breugel, W., Spinrad, H., and Djorgovski, S. A correlation between the radio and optical morphologies of distant 3Cr radio galaxies. *ApJ*, 321:L29–L33, Oct. 1987. doi: 10.1086/185000.

McCarthy, P. J., Spinrad, H., Dickinson, M., et al. Extended Ly-alpha emission associated with 3C 294. *ApJ*, 365:487–501, Dec. 1990. doi: 10.1086/169503.

McCarthy, P. J., Spinrad, H., and van Breugel, W. Emission-Line Imaging of 3CR Radio Galaxies. I. Imaging Data. *ApJS*, 99:27, July 1995. doi: 10.1086/192178.

Miley, G., Carilli, C., Taylor, G. B., de Breuck, C., and Cohen, A. High Redshift Radio Galaxies: Laboratories for Massive Galaxy and Cluster Formation in the early Universe. *ArXiv e-prints*, Feb. 2009.

Nagao, T., Maiolino, R., and Marconi, A. Gas metallicity in the narrow-line regions of high-redshift active galactic nuclei. *A&A*, 447:863–876, Mar. 2006. doi: 10.1051/0004-6361:20054127.

Nesvadba, N. P. H., Lehnert, M. D., Eisenhauer, F., et al. Extreme Gas Kinematics in the z=2.2 Powerful Radio Galaxy MRC 1138-262: Evidence for Efficient Active Galactic Nucleus Feedback in the Early Universe? *ApJ*, 650:693–705, Oct. 2006. doi: 10.1086/507266.

Nesvadba, N. P. H., Lehnert, M. D., Genzel, R., et al. Intense Star Formation and Feedback at High Redshift: Spatially Resolved Properties of the z = 2.6 Submillimeter Galaxy SMM J14011+0252. *ApJ*, 2007.

Nesvadba, N. P. H., Lehnert, M. D., De Breuck, C., Gilbert, A. M., and van Breugel, W. Evidence for powerful AGN winds at high redshift: dynamics of galactic outflows in radio galaxies during the "Quasar Era". *A&A*, 491:407–424, Nov. 2008. doi: 10.1051/0004-6361:200810346.

Nesvadba, N. P. H., Neri, R., De Breuck, C., et al. CO line emission in the halo of a radio galaxy at z = 2.6. *MNRAS*, 395:L16–L20, May 2009. doi: 10.1111/j.1745-3933.2009.00631.x.

Neufeld, D. A. The transfer of resonance-line radiation in static astrophysical media. *ApJ*, 350:216–241, Feb. 1990. doi: 10.1086/168375.

Oke, J. B., Cohen, J. G., Carr, M., et al. The Keck Low-Resolution Imaging Spectrometer. *PASP*, 107:375, Apr. 1995. doi: 10.1086/133562.

Pentericci, L., Röttgering, H. J. A., Miley, G. K., et al. HST images and properties of the most distant radio galaxies. *A&A*, 341:329–347, Jan. 1999.

Pentericci, L., Van Reeven, W., Carilli, C. L., Röttgering, H. J. A., and Miley, G. K. VLA radio continuum observations of a new sample of high redshift radio galaxies. *A&AS*, 145:121–159, July 2000. doi: 10.1051/aas:2000104.

Pentericci, L., McCarthy, P. J., Röttgering, H. J. A., et al. NICMOS Observations of High-Redshift Radio Galaxies: Witnessing the Formation of Bright Elliptical Galaxies? *ApJS*, 135:63–85, July 2001. doi: $10.1086/321781$.

Reuland, M., van Breugel, W., Röttgering, H., et al. Giant Lyα Nebulae Associated with High-Redshift Radio Galaxies. *ApJ*, 592:755–766, Aug. 2003. doi: $10.1086/375619$.

Robinson, A., Binette, L., Fosbury, R. A. E., and Tadhunter, C. N. Emission-line activity in radio galaxies. *MNRAS*, 227:97–114, July 1987.

Rocca-Volmerange, B., Le Borgne, D., De Breuck, C., Fioc, M., and Moy, E. The radio galaxy K-z relation: The 10^{12} $M_{\odot}$ mass limit. Masses of galaxies from the L_K luminosity, up to z $>$ 4. *A&A*, 415:931–940, Mar. 2004. doi: $10.1051/0004\text{-}6361{:}20031717$.

Röttgering, H. and Pentericci, L. Lyα emitting gas in distant radio galaxies: an evolutionary probe? In Röttgering, H. J. A., Best, P. N., and Lehnert, M. D., editors, *The Most Distant Radio Galaxies*, page 85, 1999.

Röttgering, H. J. A. *Ultra-steep spectrum radio sources: tracers of distant galaxies*. PhD thesis, Ph. D. thesis, University of Leiden (1993), 1993.

Röttgering, H. J. A., Lacy, M., Miley, G. K., Chambers, K. C., and Saunders, R. Samples of ultra-steep spectrum radio sources. *A&AS*, 108:79–141, Nov. 1994.

Röttgering, H. J. A., Hunstead, R. W., Miley, G. K., van Ojik, R., and Wieringa, M. H. Spatially Resolved Lyman-Alpha Absorption in the Z=2.9 Radio Galaxy 0943-242. *MNRAS*, 277: 389, Nov. 1995.

Röttgering, H. J. A., van Ojik, R., Miley, G. K., et al. Spectroscopy of ultra-steep spectrum radio sources: a sample of z$>$2 radio galaxies. *A&A*, 326:505–527, Oct. 1997.

Saikia, D. J., Jeyakumar, S., Wiita, P. J., Sanghera, H. S., and Spencer, R. E. Compact steep-spectrum radio sources and unification schemes. *MNRAS*, 276:1215–1223, Oct. 1995. doi: $10.1093/\mathrm{mnras}/276.4.1215$.

Saripalli, L., Hunstead, R. W., Subrahmanyan, R., and Boyce, E. A Complete Sample of Megaparsec-sized Double Radio Sources from the Sydney University Molonglo Sky Survey. *AJ*, 130:896–922, Sept. 2005. doi: $10.1086/432507$.

Scheuer, P. A. G. Models of extragalactic radio sources with a continuous energy supply from a central object. *MNRAS*, 166:513–528, Mar. 1974.

Seymour, N., Stern, D., De Breuck, C., et al. The Massive Hosts of Radio Galaxies across Cosmic Time. *ApJS*, 171:353–375, Aug. 2007. doi: $10.1086/517887$.

Shapley, A. E., Steidel, C. C., Pettini, M., and Adelberger, K. L. Rest-Frame Ultraviolet Spectra of z $\sim$ 3 Lyman Break Galaxies. *ApJ*, 588:65–89, May 2003. doi: $10.1086/373922$.

Silk, J. and Rees, M. J. Quasars and galaxy formation. *A&A*, 331:L1–L4, Mar. 1998.

Sparke, L. S. and Gallagher, J. S. *Galaxies in the Universe: An Introduction*. Cambridge University Press, 2007.

Spearman, C. *The Proof and Measurement of Association between Two Things*. University of Illinois Press, 1904.

Spergel, D. N., Verde, L., Peiris, H. V., et al. First-Year Wilkinson Microwave Anisotropy Probe (WMAP) Observations: Determination of Cosmological Parameters. *ApJS*, 148: 175–194, Sept. 2003. doi: $10.1086/377226$.

Springel, V., White, S. D. M., Jenkins, A., et al. Simulations of the formation, evolution and clustering of galaxies and quasars. *Nature*, 435:629–636, June 2005. doi: $10.1038/\mathrm{nature03597}$.

Tadhunter, C. N. High-velocity gas in powerful radio galaxies. *MNRAS*, 251:46P–50P, Aug. 1991.

Tadhunter, C. N., Scarrott, S. M., Draper, P., and Rolph, C. The optical polarizations of high- and intermediate-redshift radio galaxies. *MNRAS*, 256:53P–58P, June 1992.

Tadhunter, C. N., Villar-Martin, M., Morganti, R., Bland-Hawthorn, J., and Axon, D. The large-scale distribution of warm ionized gas around nearby radio galaxies with jet-cloud interactions. *MNRAS*, 314:849–857, June 2000. doi: $10.1046/\mathrm{j.1365\text{-}8711.2000.03416.x}$.

Tody, D. IRAF in the Nineties. In Hanisch, R. J., Brissenden, R. J. V., and Barnes, J., editors, *Astronomical Data Analysis Software and Systems II*, volume 52 of *Astronomical Society of the Pacific Conference Series*, page 173, Jan. 1993.

van Ojik, R. PhD thesis, PhD Thesis, Sterrewacht Leiden, 1995.

van Ojik, R., Rottgering, H. J. A., Miley, G. K., et al. TX0211-122: A starburst radio galaxy at z = 2.34? *A&A*, 289:54–60, Sept. 1994.

van Ojik, R., Roettgering, H. J. A., Carilli, C. L., et al. A powerful radio galaxy at z=3.6 in a giant rotating Lyman α halo. *A&A*, 313:25–44, Sept. 1996.

van Ojik, R., Roettgering, H. J. A., Miley, G. K., and Hunstead, R. W. The gaseous environments of radio galaxies in the early Universe: kinematics of the Lyman α emission and spatially resolved H I absorption. *A&A*, 317:358–384, Jan. 1997.

Venemans, B. P., Röttgering, H. J. A., Overzier, R. A., et al. Discovery of six Lyα emitters near a radio galaxy at z $\sim$ 5.2. *A&A*, 424:L17–L20, Sept. 2004. doi: $10.1051/0004\text{-}6361:200400041$.

Vernet, J., Fosbury, R. A. E., Villar-Martín, M., et al. Radio galaxies at z $\sim$ 2.5: Results from Keck spectropolarimetry. *A&A*, 366:7–25, Jan. 2001. doi: $10.1051/0004\text{-}6361:20000076$.

Villar-Martín, M., Tadhunter, C., and Clark, N. The ionization mechanism of the extended gas in high redshift radio galaxies: shocks or AGN photoionization? *A&A*, 323:21–30, July 1997.

Villar-Martín, M., Fosbury, R. A. E., Binette, L., Tadhunter, C. N., and Rocca-Volmerange, B. UV rest frame spectroscopy of four high redshift (z>2) active galaxies. *A&A*, 1999a.

Villar-Martín, M., Tadhunter, C., Morganti, R., Axon, D., and Koekemoer, A. PKS 2250-41 and the role of jet-cloud interactions in powerful radio galaxies. *MNRAS*, 1999b.

Villar-Martín, M., Fosbury, R., Vernet, J., et al. Gas metallicities and early evolution of distant radio galaxies. *Astrophysics and Space Science Supplement*, 277:571–574, 2001. doi: $10.1023/\text{A:}1012764309451$.

Villar-Martín, M., Vernet, J., di Serego Alighieri, S., et al. Giant low surface brightness haloes in distant radio galaxies: USS0828+193. *MNRAS*, 336:436–444, Oct. 2002. doi: $10.1046/\text{j.}1365\text{-}8711.2002.05751.\text{x}$.

Villar-Martín, M., Vernet, J., di Serego Alighieri, S., et al. Kinematically quiet haloes around z $\sim$ 2.5 radio galaxies. Keck spectroscopy. *MNRAS*, 346:273–294, Nov. 2003. doi: $10.1046/\text{j.}1365\text{-}2966.2003.07090.\text{x}$.

Villar-Martín, M., Sánchez, S. F., De Breuck, C., et al. VIMOS-VLT and Spitzer observations of a radio galaxy at z= 2.5*. *MNRAS*, 366:L1–L5, Feb. 2006. doi: $10.1111/\text{j.}1745\text{-}3933.2005.00118.\text{x}$.

Willott, C. J., Rawlings, S., Jarvis, M. J., and Blundell, K. M. Near-infrared imaging and the K-z relation for radio galaxies in the 7C Redshift Survey. *MNRAS*, 339:173–188, Feb. 2003. doi: $10.1046/\text{j.}1365\text{-}8711.2003.06172.\text{x}$.

Zirm, A. W., Overzier, R. A., Miley, G. K., et al. Feedback and Brightest Cluster Galaxy Formation: ACS Observations of the Radio Galaxy TN J1338-1942 at z = 4.1. *ApJ*, 630: 68–81, Sept. 2005. doi: 10.1086/431921.